Unterschrift Betreuer

TU WIEN
TECHNISCHE UNIVERSITÄT WIEN

DIPLOMARBEIT

Investigation of different detection approaches for measurement of blood flow velocities in retinal vessels of rodents

ausgeführt am Institut für
Angewandte Physik (E 134)
der Technischen Universität Wien

in Zusammenarbeit mit dem

Zentrum für Medizinische Physik und Biomedizinische Technik
der Medizinischen Universität Wien

unter der Anleitung von

Ao.Univ.-Prof. DI Dr. Martin Gröschl

(Technische Universität Wien)

Ao. Univ.-Prof. DI Dr. Leopold Schmetterer
Assoc. Prof. DI(FH) René Werkmeister, PhD

(Medizinische Universität Wien)

durch

Thomas Blaschke, BSc

Hauptstraße 5/2/8
A-3001 Mauerbach

Wien, 13.09.2017

Ort, Datum

Unterschrift Student

Abstract

There are several ocular diseases adduced by the World Health Organisation most responsible for causing loss in the field of vision. Some of them can be linked to the status of the ocular blood flow in retinal blood vessels, which makes parameters defining the blood flow an important and interesting field of research.

Laser Doppler Velocimetry is a non-invasive and cheap measurement technique aiming to measure the blood flow velocity either relative, with a single detector system or absolute, with the incorporation of a second detector.

The development, progression and possible treatment of diseases are often studied with the use of animal models. Statistics show that rats are often used in animal experiments, especially for the research of the ocular system. Over the years, researchers have developed several different rodent models for ocular diseases. Therefore, it is useful to build a measurement system for the use of Laser Doppler Velocimetry adapted to their anatomical needs.

In this thesis, a single detector laser Doppler flowmeter and its data acquisition program, provided by the cooperating Institute of Systems Engineering from the HES-SO Valais-Wallis in Sion, Switzerland, is changed and used for Laser Doppler Velocimetry measurements. The changed single detector system is used to find out, if the anatomy of the rat eye allows the measurement of the absolute velocity of blood flow in retinal blood vessels via a measurement system with two detectors.

The measurement system and the changed data acquisition program were evaluated with in vitro measurements on a rotating disc and a glass capillary. The made measurement results of both measurement setups confirm a strong correlation to theoretical Laser Doppler Velocimetry calculations. An interpretation of the measurement results of the glass capillary setup indicates that a measurement system capable of measuring the absolute velocity of blood flow in retinal blood vessels in rat eyes should be realisable.

Kurzfassung

Die Weltgesundheitsorganisation weist einigen Augenkrankheiten die Hauptverant-
wortung für Verluste im Blickfeld zu. Manche dieser Krankheiten können mit dem
Zustand des Blutflusses in den retinalen Blutgefäßen im Auge in Zusammenhang
gebracht werden. Diese Tatsache macht die Untersuchung der Parameter des Blut-
flusses zu einem wichtigen und interessanten Forschungsgebiet.

Die Laser Doppler Velocimetry ist eine kontaktlose, schmerzfreie und relativ billige
Messmethode, die es zum Ziel hat, die Geschwindigkeit des Blutflusses festzustellen.
Mit einem Messsystem, welches nur einen Detektor beinhaltet, kann die relative
Blutflussgeschwindigkeit festgestellt werden, mit einem zweiten Detektor kann das
Messsystem die absolute Blutflussgeschwindigkeit messen.

Der Verlauf und mögliche Behandlungsmethoden von Krankheiten werden oft mit
dem Einsatz von Tiermodellen untersucht. Wie die Tierversuchsstatistik zeigt, wer-
den Ratten oft als Versuchstiere für Forschungszwecke verwendet und gerade für
Untersuchungen des visuellen Systems herangezogen. Im Laufe der Jahre haben
Forscher verschiedene Tiermodelle für Nagetiere entwickelt, um Augenkrankheiten
untersuchen zu können. Daher ist es sinnvoll, ein Messsystem aufzubauen, das für
Laser Doppler Velocimetry Messungen am Rattenauge geeignet ist. Dabei muss vor
allem auf die Unterschiede in der Anatomie zwischen dem Auge des Menschen und
dem der Ratte geachtet werden.

Für diese Arbeit werden ein Laser Doppler Flowmeter und das dazugehörige Da-
tenerfassungsprogramm, welches vom Institut der Systemtechnik der Hochschule
HES-SO Valais-Wallis (Sion, Schweiz) zur Verfügung gestellt wurde, so abgeändert,
dass Laser Doppler Velocimetry Messungen möglich werden. Das abgeänderte Mess-
system besitzt einen Detektor und soll dazu verwendet werden, herauszufinden, ob
sich ein Messsystem mit zwei Detektoren bauen lässt, das auf die Anatomie der
Ratte eingeht und die Messung der absoluten Blutflussgeschwindigkeit in retinalen
Blutgefäßen des Rattenauges ermöglicht.

Das abgeänderte Messsystem und das dazugehörige Datenerfassungsprogramm wer-
den mit in vitro Messungen an einer sich drehenden Scheibe und einer blutdurch-
flossenen Glaskapillare getestet. Die erhaltenen Messergebnisse beider Versuchsauf-

bauten stimmen gut mit den theoretisch errechneten Ergebnissen der Laser Doppler Velocimetry überein. Wenn man die Ergebnisse des zweiten Versuchsaufbaus interpretiert, stellt man fest, dass ein Messsystem gebaut werden kann, welches die absolute Geschwindigkeit des Blutflusses in retinalen Blutgefäßen im Rattenauge misst.

Acknowledgements

Contents

List of figures

1

3

4

List of tables

List of abbreviations

WHO World Health Organisation

LDV Laser Doppler Velocimetry

RBC red blood cell

RBCs red blood cells

LD laser diode

SLD superluminescent diode

LED light emitting diode

PMT photomultiplier tube

APD avalanche photodiode

OMS optical mixing spectroscopy

DSPS Doppler shift power spectrum density

DC direct current

LDF Laser Doppler Flowmetry

CCD charge-coupled device

PCI peripheral component interconnect

DAQ data acquisition

VI virtual instrument

IOP intra ocular pressure

AI analogue input

OCT optical coherence tomography

MAE mean absolute error

1. Introduction

There are ocular diseases, like cataract, onchocerciasis, childhood blindness, refractive errors and low vision, diabetic retinopathy, glaucoma, age-related macular degeneration and corneal opacities and genetic eye diseases that are named by the World Health Organisation (WHO) most responsible for causing loss in the field of vision or even blindness [4]. Even though their pathophysiology is still not fully understood, some of them, like diabetic retinopathy, glaucoma and age-related macular degeneration, can be linked to the status of the ocular blood flow in the retinal vessels of the eye [5–7]. Therefore, every parameter defining the blood flow is in the focus of interest and a lot of research is put into different measurement methods measuring the blood flow and its parameters [8–10].

Laser Doppler Velocimetry (LDV) is aiming to measure one of these parameters non-invasively that is already revealed in the name, the velocity of the blood flow. The biggest advantage of this measuring method is the cheap hardware used in the measurement system. Furthermore, a LDV system using two detectors can measure not only the relative, but the absolute velocity of the blood flow.

The method of LDV has its foundation in 1964. Over the years it has become a very versatile measurement technique which is used for many other applications, e.g. the characterization of nano particles or the accurate detection of a vehicles velocity [11, 12].

Animal models are often used to investigate diseases and help to gain an insight into their development, progression and possible treatment. To research diseases under controlled conditions, animal experiments are used. In the statistic of animal experiments done in Austria, rats rank in either place three or four in numbers of subjects over at least the last 17 years [13]. Over the years, researchers have developed several different rodent models for ocular diseases. The transparent eye is the ideal sample to determine parameters of the blood flow. Therefore, it is useful to build a measurement system for the use of Laser Doppler Velocimetry adapted to their anatomical needs.

The thesis is in cooperation with the Institute of Systems Engineering from the HES-SO Valais-Wallis in Sion, Switzerland, which provides the measurement system (hardware and data acquisition (DAQ) program) that is the basis of this work [14]. This single detector measurement system is a compact laser Doppler flowmeter fundus camera for the assessment of retinal blood perfusion in small animals that

was built by M. Mentek et al. [3].

Using this single detector laser Doppler flowmeter as starting point, the goal of this thesis is, to find out the possibility of measuring the absolute velocity of blood flow in retinal blood vessels of rat eyes via a LDV system with two detectors.

2. The rat eye

Rat eyes have similar characteristics, function and structure as all mammals. Nevertheless, there are some important differences between rat and human eyes regarding LDV measurements.

One optical difference is the transmitted range of wavelengths. While the lens of a humans eye transmits only visible light, a lens of a rat eye is able to transmit almost 50% of ultraviolet A light as well [15].

The ratio of the lens size to the whole eyeball of the rat is bigger compared to the same ratio in human eyes. This fact is shown in Fig. 2.1, a ZEMAX illustration comparing a human to a rat eye.
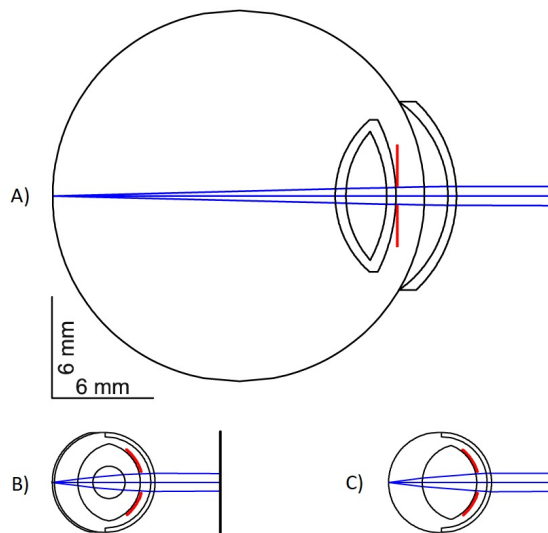
Figure 2.1: Relaxed schematic eyes in ZEMAX. A) Gullstrand's human schematic eye B) Hughes' schematic rat eye and C) is the reduced schematic rat eye (rSRE). All eyes show a pupil diameter of 1 mm (red lines) (adapted from Link et al. [1]).

The rat eye has an axial length of only 6.29 ± 0.007 mm (in comparison humans have an axial eye length of ~ 24 mm) [16, 17]. As the human eye, the pupil of the rat eye is highly variable in size. The pupil diameter of a rat eye can vary between $0.2 - 1.2$ mm (these extreme diameters can be measured under bright or

dim light) [18]. During optical measurements in the eye, it is common to dilate the eyes pupil to make it unresponsive to light signals and reproducible measurements can be done. Therefore, a maximum pupil diameter has to be taken into account for LDV measurements.
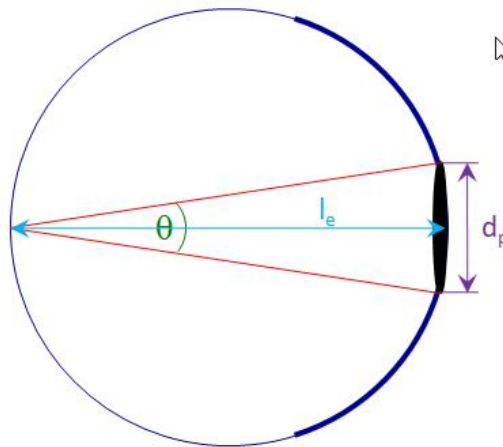
Figure 2.2: Schematic rat eye with parameters for calculating the maximum entrance angle.

As depicted in Fig. 2.2, the maximum entrance angle θ can be calculated from the axial length l_e and the pupil diameter d_p with

$$tan\left(\frac{\theta}{2}\right) = \frac{\frac{d_p}{2}}{l_e} = \frac{d_p}{2l_e}$$

$$\implies \theta = 2 \cdot arctan\left(\frac{d_p}{2 \cdot l_e}\right)$$

$$= 2 \cdot arctan\left(\frac{1.2}{2 \cdot 6.29}\right) \approx 11°. \tag{2.1}$$

The red blood cells (RBCs) of a rat have a diameter of 6.29 ± 0.4 µm and are smaller than those of humans (7.4 ± 0.6 µm) [19]. Retinal vessels in the rat's vascular system have a diameter starting at 4.4 µm for small capillaries up to 50 µm for major arterioles and venules [20, 21]. The velocity of RBCs in retinal vessels depends on the vessel diameter. It varies from a mean velocity of ~ 3 mm/s in retinal capillaries up to a mean velocity of ~ 16 mm/s in retinal arteries [19].
The parameters collected in this chapter are necessary for LDV measurements and used in the following chapters.

3. Principles of Laser Doppler Velocimetry

Based on the Doppler effect LDV measures the velocity of a moving reflecting target (e.g. a red blood cell (RBC) in the retinal vessels of the eyes). A single detector system allows the measurement of the relative velocity, while a system with two detectors is able to provide the absolute velocity of a moving reflecting target [22]. In the following, the theoretical concepts of the main parts of LDV are described separately and afterwards these are combined to the measurement of the absolute velocity of blood flow in retinal vessels via Laser Doppler Velocimetry.

3.1 Optical imaging method with interferometry

An optical imaging method uses a light source (for example a laser, laser diode (LD) or superluminescent diode (SLD)) and detects the light scattered by a sample. As mentioned before, LDV is an optical imaging method measuring the frequency of backscattered laser light from moving reflecting targets. The speed of light is approximately $3 \cdot 10^8$ m/s. Since the RBCs of a rat have a diameter of ~ 6.3 µm, direct measurement of echo time delay would need a time resolution of $t = \frac{s}{v} \sim \frac{6.3 \cdot 10^{-6} \text{ m}}{3 \cdot 10^8 \text{ m/s}} \sim 21$ fs ($= 21 \cdot 10^{-15}$ s) (see Chap. 2) [19]. This kind of time resolution is not possible to reach with direct electronic detection and therefore, as alternative, interferometry is used ([23] p.7).

3.1.1 Michelson interferometer

The Michelson interferometer is a basic interferometer (Fig. 3.1). A beam of light is emitted by a laser light source and gets divided into two parts by a beam splitter. One part of the beam is deflected by the beam splitter and follows the y-axis, where it gets reflected by a reference mirror. The distance between beam splitter and reference mirror has the known length d_{br}. This part is called the reference beam
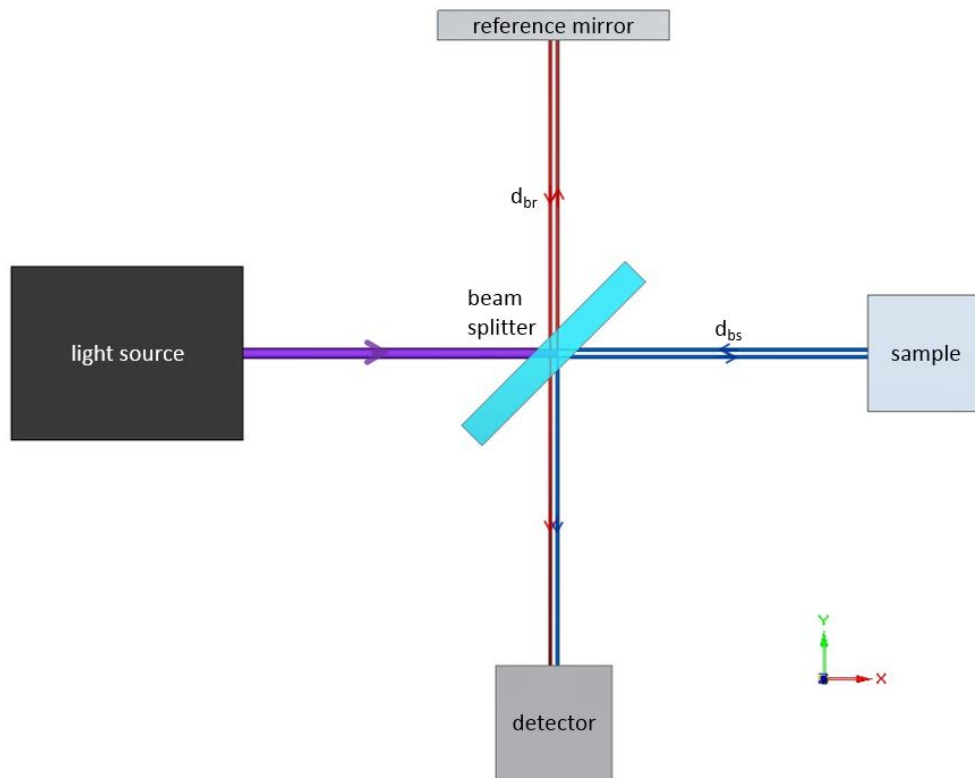
Figure 3.1: Basic principle of a Michelson interferometer

(reference arm). The reference beam is then transmitted through the beam splitter and reaches the detector surface.

The second part of the initial beam is transmitted through the beam splitter, follows the x-axis until it gets reflected by a sample, which is the intended object of the measurement. This part is called the sample beam (sample arm). The sample beam is then deflected by the beam splitter and reaches the detector surface, where it interferes with the reference beam.

The electric field of the incident beam coming from the light source is a plane wave

$$\vec{E}_i(\vec{k}, t) = A_0(\vec{k}, t) \cdot cos(\vec{k}\vec{x} - \omega t), \tag{3.1}$$

with the amplitude $A_0(\vec{k}, t)$ and the phase of $(\vec{k}\vec{x} - \omega t)$. The intensity of the plane wave is

$$I_i(\vec{k}, t) = |\vec{E}_i(\vec{k}, t)|^2. \tag{3.2}$$

Since the electric field of the incident beam is a plane wave, both beam parts are plane waves as well, where $\vec{E}_R(\vec{k}_D, t)$ is the electric field of the reference arm and $\vec{E}_S(\vec{k}_D, t)$ is the electric field of the sample arm. If the surface of the detector is big enough to receive all the light coming from the sample and the reference arm, the

combined electric field measured in the detector is ([2] p.125)

$$\vec{E}_D(\vec{k}_D, t) = \vec{E}_R(\vec{k}_D, t) + \vec{E}_S(\vec{k}_D, t). \tag{3.3}$$

The combined intensity of the reference and the sample arm measured in the detector is ([23] p.10)

$$I_D \propto |\vec{E}_R|^2 + |\vec{E}_S|^2 + 2\vec{E}_R\vec{E}_S \cdot cos\,(2k_D\Delta L), \tag{3.4}$$

where k_D is the wavenumber ($k_D = \frac{2\pi}{\lambda}$, λ ... wavelength) and $\Delta L = |d_{bs} - d_{br}|$ is the path length difference between the signal and reference arm of the interferometer (for a mathematical derivation see [24] p.18-24).
On one hand if the path length difference ΔL is changed, the Michelson interferometer can be used as a very exact device for wavelength determination. For example, if the reference mirror is mounted on a movable sliding carriage and moved continuously along the y-axis (Fig. 3.1), the intensity maxima in the detector plane can be measured and counted through photodetectors. If there are N interference maxima during the displacement of Δy, the wavelength is $\lambda = 2\Delta y/N$ ([25] p.314).
On the other hand, different wavenumbers k_D (or different wavelengths λ) change the intensity pattern. With using a source with a broad bandwidth (i.e. different wavelengths) and detecting those changes through photodetectors, the path length difference ΔL can be determined.

3.1.2   Laser diode as signal source

A LD is a light source that produces optical radiation with two important properties: a high output power and a high spatial coherence [26].
For some optical components used in a system for optical detection, a loss of intensity has to be expected. If additionally sample reflectivity is low, a bright LD as light source is needed.
The high spatial coherence provides a fixed phase relationship between the electric fields of the reference and the sample arm [27]. Consequently, the detected intensity only depends on the wavenumber k_D and the path length difference ΔL.
The coherence length is the distance in which the phase of the signal is predictable. It is inversely proportional to the frequency bandwidth of the used light source ([23] p.11). An interference pattern only appears, if the reference arm (d_{br}) and the sample arm (d_{bs}) match their distances within one coherence length.
The fixed phase relationship of the reference and the sample arm is modified by a moving target via the Doppler effect.

3.2   Doppler effect

The Doppler effect was first described by the Austrian physicist Christian Doppler in 1842. It describes the frequency shift of a wave (light or sound), that occurs, if the wave is emitted from a source moving towards or away from an observer. A typical example is the increased pitch of the siren of an ambulance upon arrival and its decreased pitch while driving away ([2] p.124).
With the signal source at rest and an observer that is moved with velocity v, the incident frequency f_0 is shifted to the Doppler frequency f_{DO} ([28] p.401)

$$f_{DO} = f_0 \left(1 \pm \frac{v}{c}\right), \tag{3.5}$$

where c is the speed of light. The upper sign has to be used, if the observer moves towards the source and the lower sign, if the observer moves away from the source. Is, however, the observer at rest and the source is moving with the velocity v, then the incident frequency f_0 is shifted to the Doppler frequency f_{DS} ([28] p.401)

$$f_{DS} = f_0 \left(\frac{1}{1 \mp \frac{v}{c}}\right). \tag{3.6}$$

Here, the upper sign has to be used if the source moves towards the observer and the lower sign if the source moves away from the observer.
In case the source as well as the observer are moving with the same velocity v, both formulas are combined to ([28] p.401)

$$f_D = f_0 \left(\frac{1 \pm \frac{v}{c}}{1 \mp \frac{v}{c}}\right). \tag{3.7}$$

The upper sign has to be used, if the source and the observer are moving towards one another and the lower sign, if they move away from one another. If $v << c$, the ratio between the velocity v and the speed of light c is very small. Thus making the denominator ≈ 1 (since it is not multiplied with f_0) and Eq. (3.7) can be simplified to

$$f_D = f_0 \left(1 \pm \frac{v}{c}\right). \tag{3.8}$$

3.3   Laser Doppler Velocimetry

Velocimetry is the measurement of the velocity of fluids. A common way to do so is through measuring the velocity of particles suspended in the fluid. The use of this measurement technique started in 1964 with measuring the velocity of polystyrene spheres of diameter 0.557 μm placed in water [29].

3.3.1   Optical imaging method in a retinal blood vessel

A velocimeter with a coherent light source as a signal source is an optical imaging method, capable of measuring the velocity of small particles suspended in a fluid. Since it uses a light source, a direct electronic detection is not working, but an interferometric approach can be used (see/compare 3.1.1).
Like in a Michelson interferometer, a beam of light is emitted from a coherent light source and gets divided into two parts by a beam splitter. Since the absolute velocity of blood flow in retinal blood vessels of rodents is the focus of interest in this thesis, a rat's eye is the sample in the sample arm of the interferometer (Fig. 3.2).
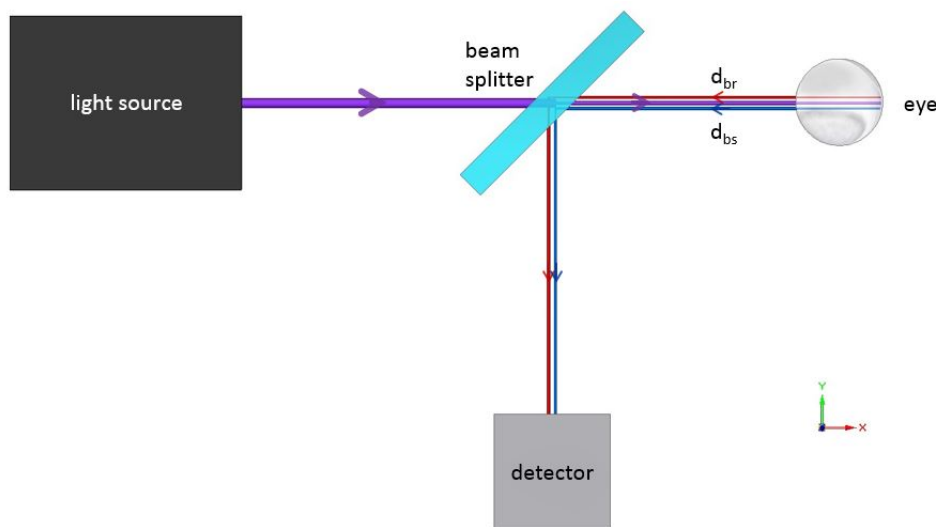
Figure 3.2: Optical imaging method (LDV) with an eye as sample.

More precisely, the RBCs in the blood stream in the targeted retinal vessel reflect part of the beam which serves as the sample beam (sample arm) (Fig. 3.3). The RBCs of rats are small and thus not all of the incident laser beam is reflected by RBCs [19]. The part of the beam that passes the RBCs is reflected by the vessel wall and serves as the reference beam.

Since RBCs are much smaller than the blood vessel, all the RBCs in the measured blood vessel form a parabolic velocity profile. According to Poiseuille's law, due to friction the velocity is zero at the vessel wall ($v = 0$), and goes up to a maximum velocity ($v = v_{max}$) in the center of the vessel (Fig. 3.4) ([2] p.125)

$$v(R) = v_{max} \cdot \left[1 - \left(\frac{R}{R_0} \right)^2 \right] . \tag{3.9}$$

In Fig. 3.4, $\vec{E}_0(\vec{k}_i, t) \cdot cos(\omega_0 t)$ is the incident electric field coming from the light
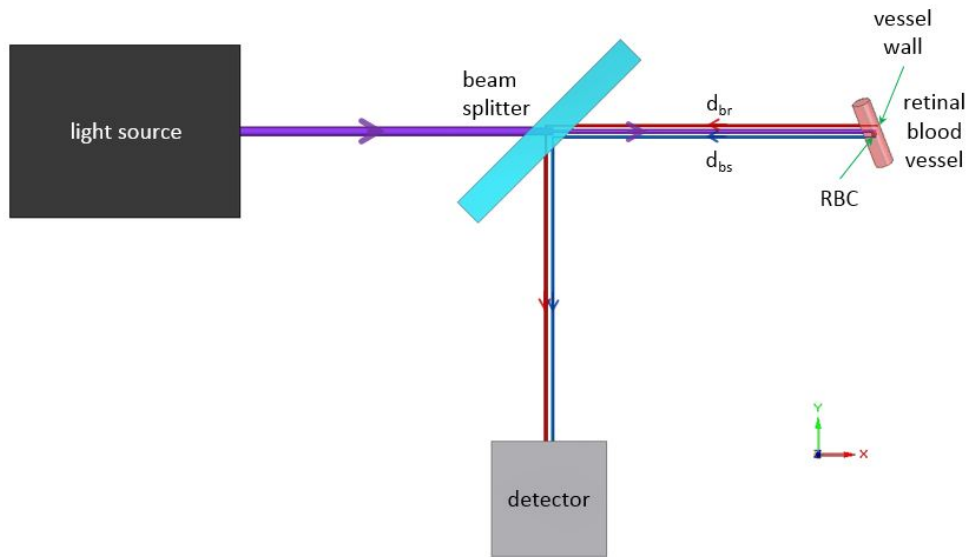
Figure 3.3: LDV in retinal blood vessels: RBCs serve as sample arm and the vessel wall as reference arm.
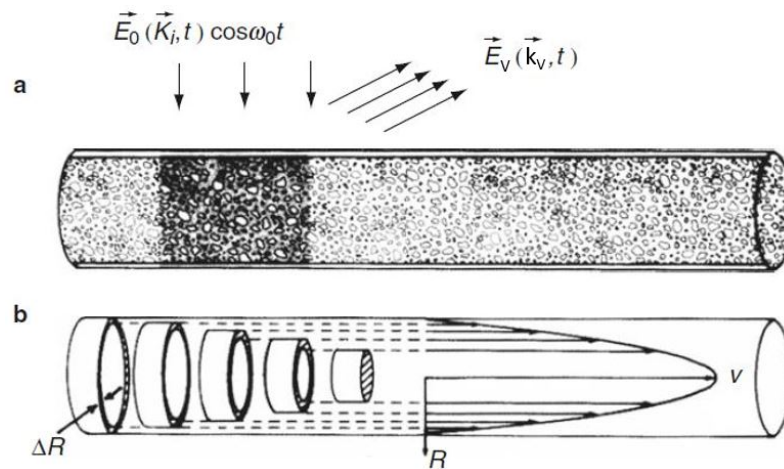
Figure 3.4: (a) Schematic representation of an incident beam $\vec{E}_0(\vec{K}_i, t)$ with wave vector $\vec{K}_i$ illuminating a volume of a capillary tube. From the tube and the moving RBCs in the tube the incident light is scattered and measured in a detector. The electric field scattered from the blood vessel (the vessel wall and the RBCs) is $\vec{E}_V(\vec{k}_V, t)$ dependent on the wave vector $\vec{k}_V$ (b) assumed parabolic velocity profile of RBCs in a blood vessel. The velocity V obeys Poiseuilles's law (adapted from Riva and Feke [2] p.125).

source encountering the blood vessel. The electric field coming from the reference arm is the non-shifted electrical field $\vec{E}_R(\vec{k}_V, t)$ from the vessel wall (in literature also called $\vec{E}_{LO}(\vec{k}_V, t)$, where "LO" stands for "local oscillator"). The electric field of the sample beam consists of several different electrical fields $\vec{E}_{Si}(\vec{k}_V, t)$ (where i is the index), one for each moving RBC. If the blood vessel is subdivided into N parts of different velocities, reaching from zero at the vessel wall ($v = 0$) up to the maximum velocity ($v = v_{max}$), the time-dependent equation for the electric field scattered from the blood vessel $\vec{E}_V(\vec{k}_V, t)$ Eq. (3.3) may be written as ([2] p.125)

$$\vec{E}_V(\vec{k}_V, t) = \vec{E}_R(\vec{k}_V, t) + \sum_{i=0}^{N} \vec{E}_{Si}(\vec{k}_V, t), \qquad (3.10)$$

where $\vec{k}_V$ is the wave-vector in the scattering direction.

3.3.2 Relative velocity of red blood cells in a retinal blood vessel

Each moving RBC inflicts a Doppler shift upon the electrical field, depending on the RBC's speed. The time-dependent electrical fields of the reference beam $\vec{E}_R(\vec{k}_V, t)$ (from the vessel wall) and the sample beam $\vec{E}_{Si}(\vec{k}_V, t)$ (from RBCs) can be written as

$$\vec{E}_R(\vec{k}_V, t) = A_R(\vec{k}_V) \cdot cos\,(2\pi f_0 t)$$
$$\vec{E}_{Si}(\vec{k}_V, t) = A_{Si}(\vec{k}_V) \cdot cos\,[2\pi\,(f_0 + \Delta f_i)\,t]\,. \qquad (3.11)$$

In Eq. (3.11), $A_R(\vec{k}_V)$ is the amplitude of the reference beam reflected by the vessel wall, f_0 is the incident (non-shifted) frequency, $A_{Si}(\vec{k}_V)$ are i different amplitudes for each Doppler shifted signal and Δf_i are the correlated Doppler shifted frequency differences. Under the assumption, that the volume of the measured part of the tube is uniformly illuminated by the laser and the particles in the tube have a uniform concentration across the tube, the time-dependent electric field of the sample beam $\vec{E}_{Si}(\vec{k}_V, t)$ can be simplified to

$$\vec{E}_{Si}(\vec{k}_V, t) = A_S(\vec{k}_V) \cdot cos\,[2\pi\,(f_0 + \Delta f_i)\,t] \qquad (3.12)$$

and the same amplitude $A_S(\vec{k}_V)$ can be used for all electric fields, $\vec{E}_{Si}(\vec{k}_V, t)$, scattered by RBCs. Together with the electric field from the reference arm, $\vec{E}_R(\vec{k}_V, t)$, these electric fields build the electric field $\vec{E}_V(\vec{k}_V, t)$, that is scattered from the blood vessel (see Eq. (3.10)). The scattered electric field can be written as

$$\vec{E}_V(\vec{k}_V, t) = A_R(\vec{k}_V) \cdot cos\,(2\pi f_0 t) + A_S(\vec{k}_V) \cdot \sum_{i=0}^{N} cos\,[2\pi\,(f_0 + \Delta f_i)\,t]\,. \qquad (3.13)$$

With applying Fourier analysis, the power spectral density of the scattered light from the blood vessel $P_V(f)$ can be calculated with

$$P_V(f) = \frac{A_R^2}{2} \cdot \delta(f - f_0) + \frac{A_R A_S}{2} \cdot \sum_{i=0}^{N} \delta \left[f - (f_0 + \frac{i \cdot \Delta f_{max}}{N}) \right] \qquad (3.14)$$

with $f_0 \leq f \leq f_0 + \Delta f_{max}$.

The Fourier analysis results in one delta function at the incident frequency f_0 and one for each RBC at the frequency differences $f_0 + \frac{i \cdot \Delta f_{max}}{N}$ (with $1 \leq i \leq N$).

As stated at the beginning of Chap. 3.1, direct electronic detection is not able to detect the scattered light with the frequency f, because it is still in the optical frequency range from f_0 up to $f_0 + \Delta f_{max}$ and thus to high for direct detection. With directing the scattered light onto a photomultiplier tube (PMT) (or in this case an avalanche photodiode (APD), see later), the power spectral density of the scattered light can be translated down to lower frequencies that are within the acoustic range. This technique is known as "optical mixing spectroscopy (OMS)" ([2] p.124,126). OMS relies on the evaluation of the generated photocurrent $i(\vec{r}, t)$ in the photodetector. Assuming the photodetector has a surface S, $\vec{r}$ is one point on that surface. With the responsivity β of the surface S of the photodetector, the time average of the photocurrent can be written as

$$\langle i(t) \rangle = \int_S \beta \vec{E}_D(\vec{k}_D, t) dS. \qquad (3.15)$$

This time average of the photocurrent incorporates all information on the velocities of the RBCs. This information can be extracted and leads to the Doppler shift power spectrum density (DSPS) = $P_D(\Delta f)$, in the detector

$$P_D(\Delta f) = \frac{1}{2} e \beta S \left[A_R^2 + A_S^2 \right] + \frac{1}{4} \beta^2 S^2 \left[A_R^2 + A_S^2 \right]^2 \cdot \delta(\Delta f) +$$

$$+ \beta S S_{cohD} A_R^2 A_S^2 \cdot \sum_{i=0}^{N} \delta \left(\Delta f - \frac{i \cdot \Delta f_{max}}{N} \right) \qquad \text{for } 0 \leq \Delta f \leq \Delta f_{max}$$

and

$$P_D(\Delta f) = \frac{1}{2} e \beta S \left[A_R^2 + A_S^2 \right] \qquad \qquad \text{for } \Delta f > \Delta f_{max} ,$$

$$(3.16)$$

(exact derivation see [30] p.139-143). In Eq. (3.16), e is the charge of the electron, $\Delta f = f - f_0$ is the frequency difference or beating frequency between the Doppler shifted frequency f of the light reflected by the RBCs and the frequency f_0 of the

light reflected by the vessel wall, S_{cohD} is the coherence area of the reference beam at the detector surface and Δf_{max} is the maximum frequency difference or cut-off frequency of $P_D(\Delta f)$.

The first term in Eq. (3.16), which still exists beyond the maximum frequency difference ($\Delta f > \Delta f_{max}$), is the photodetector shot noise. The shot noise signal is measured even without any signal. The second and third terms are again delta functions (compare to Eq. (3.14)). The intensity of the reference signal coming from the vessel wall is much larger than the sample signal coming from the RBCs and therefore, $A_R >> A_S$.

Comparing Eq. (3.14) and Eq. (3.16) one can see that in Eq. (3.16) the power spectrum density is depending on the frequency difference Δf instead on the frequency f of the reflected light. Therefore, the OMS procedure shifts the power spectrum density in Eq. (3.14) (which is depending on f of the reflected light) down towards lower frequencies (Δf in the range of kHz) of the Doppler shifted power spectrum in Eq. (3.16). Based on Eq. (3.16) spectral analysis with a high resolution can be performed with conventional devices. The expected DSPS ($P_D(\Delta f)$) is depicted in Fig. 3.5.
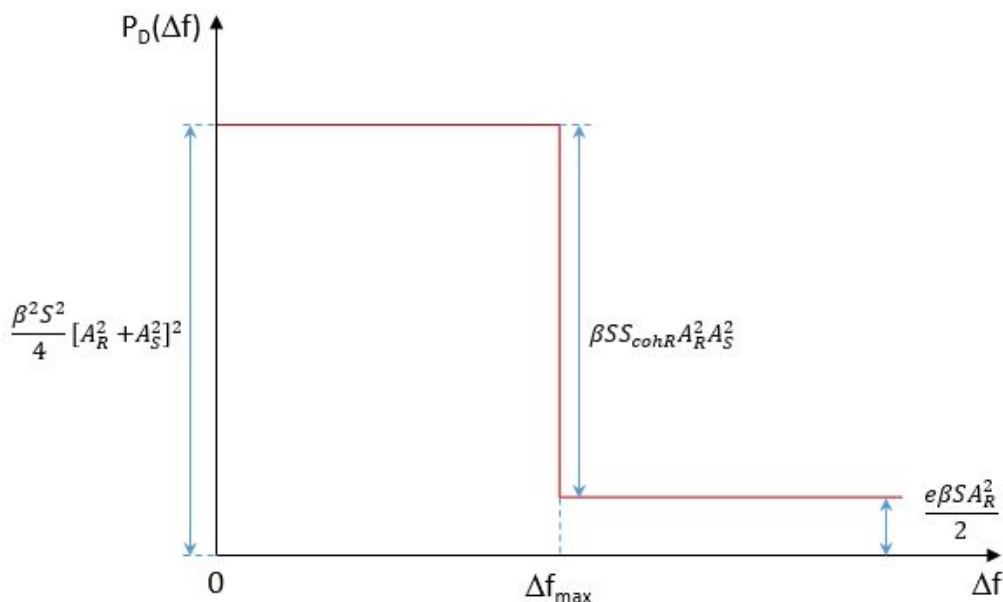
Figure 3.5: Theoretically predicted Doppler shifted power spectrum density $P_D(\Delta f)$. The parameters are: the DC component $\frac{1}{4}\beta^2 S^2 \left[A_R^2 + A_S^2\right]^2$ at $\Delta f = 0$, the sample component $\beta SS_{cohD}A_R^2 A_S^2$ in the interval $0 \leq \Delta f \leq \Delta f_{max}$ and the shot noise $\frac{1}{2}e\beta S \left[A_R^2 + A_S^2\right]$ for all Δf (adapted from Schmetterer and Kiel [2] p.127).

From the DSPS, the cut-off frequency Δf_{max} can be determined.

Using the Doppler effect Eq. (3.8), the frequency difference can be used for calcu-

lating the velocity of the RBCs.

$$\Delta f = f_D - f_0$$
$$= f_0 \cdot \left(1 \pm \frac{v}{c}\right) - f_0$$
$$= f_0 \pm f_0 \cdot \frac{v}{c} - f_0$$
$$= \pm f_0 \cdot \frac{v}{c} \tag{3.17}$$

And with the incident wavelength of the laser diode, $\lambda_0 = c/f_0$, the frequency difference is

$$\Delta f = \pm \frac{v}{\lambda_0}. \tag{3.18}$$

It is now necessary to take a closer look at the general geometry of a measurement setup.

Fig. 3.6 depicts the measurement system and a RBC moving in the direction of v_{RBC} in a blood vessel. Looking at the plan view (detailed Fig. 3.6A) one can see, that the RBC velocity can be separated in a part in the direction of the laser beam, v_x, and a part perpendicular to that, v_y. The Doppler effect measured by the detector is only caused by the velocity part v_x in axial direction of the laser beam and consequently Eq. (3.18) can be changed to

$$\Delta f = \pm \frac{v_x}{\lambda_0}. \tag{3.19}$$

The goal is to measure the velocities of RBCs in a blood vessel. The geometry can be used to get a connection between the velocity causing the Doppler effect v_x and the velocity of the RBC (v_{RBC}) in the blood vessel. Looking again at Fig. 3.6A, the velocities of the RBCs can be calculated from v_x with the simple angle relation

$$v_{RBC} = \frac{v_x}{sin(\gamma)}. \tag{3.20}$$

A direct connection to the angle between the blood vessel and the laser beam is preferable. That angle is called Doppler angle and is named δ in Fig. 3.6A. With $\gamma = \delta - 90°$ and $sin\,(x \pm y) = sin\,(x)\,cos\,(y) \pm cos\,(x)\,sin\,(y)$

$$sin(\gamma) = sin(\delta - 90°)$$
$$= sin(\delta)cos(90°) - cos(\delta)sin(90°)$$
$$= -cos(\delta) \tag{3.21}$$

and consequently

$$v_x = -v_{RBC} \cdot cos(\delta). \tag{3.22}$$
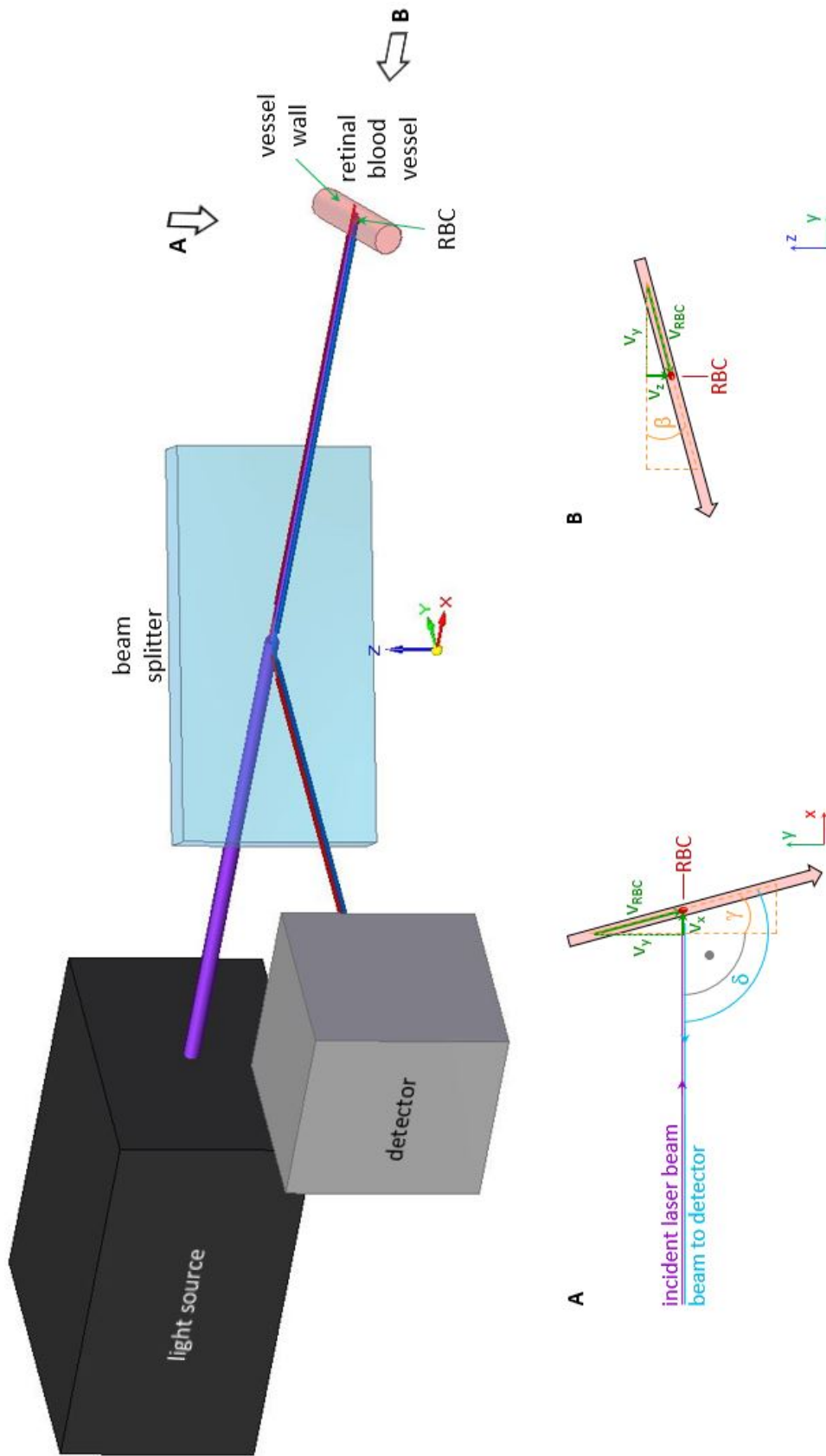
Figure 3.6: Measurement system with a moving RBC in direction of v_{RBC}. A: Plan view of vessel with one RBC. Connection of the velocity of the RBCs v_{RBC} to the part of the velocity in direction of the beam v_x and the Doppler angle δ. B: Side view of vessel with one RBC. Connection of the velocity of the RBCs v_{RBC} to the angle β.

With Eq. (3.22), the connection between the velocity of the RBC and the frequency difference of the Doppler shift can be made

$$\Delta f = \mp \frac{v_{RBC} \cdot cos(\delta)}{\lambda_0}. \tag{3.23}$$

During measurements only absolute values of Δf are measured and with the Doppler angle $90° < \delta < 180°$ the cosine function is always negative. Therefore, Eq. (3.23) can be changed to

$$|\Delta f| = \frac{v_{RBC} \cdot |cos(\delta)|}{\lambda_0}. \tag{3.24}$$

For an absolute estimation of the frequency difference, the refractive index n_b from the blood in the vessel has to be taken into account. It can be integrated in the numerator and changes Eq. (3.24) to

$$\Delta f = \frac{v_{RBC} \cdot n_b \cdot |cos(\delta)|}{\lambda_0}. \tag{3.25}$$

Therefore, the relative velocity of the RBC in the blood vessel can be calculated through the measured frequency difference of the Doppler shift with

$$v_{RBC} = \frac{\Delta f \cdot \lambda_0}{n_b \cdot |cos(\delta)|}. \tag{3.26}$$

The maximum relative velocity of the RBCs in the center of the blood vessel can be calculated through the measured maximum frequency difference (or cut-off frequency) of the Doppler shift with

$$\boxed{v_{RBC} = \frac{\Delta f_{max} \cdot \lambda_0}{n_b \cdot |cos(\delta)|}}. \tag{3.27}$$

3.3.3 Absolute velocity of red blood cells in a retinal blood vessel

The Doppler angle δ is not available, because from an en face image (i.e. a frontal image) it can not be determined, how much the blood vessel is tilted into the background. In other words, the angle γ between the y-z-plane and the blood flow velocity $\vec{v}_{RBC}$ (Fig. 3.6) can not be identified. Therefore, Eq. (3.27) only calculates the relative velocity of the RBCs, because it still depends on the undefined Doppler angle δ.
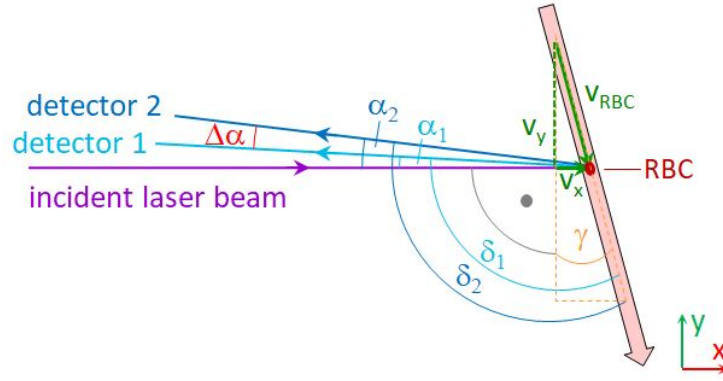
Figure 3.7: Plan view of vessel with one RBC (compare to 3.6A). Geometry of a measurement system with two detectors for measuring the absolute velocity of RBCs in a blood vessel.

To calculate the absolute velocity of RBCs in a blood vessel, a measurement system with two detectors, with a defined intraocular angle $\Delta\alpha$ between the scattering directions, is needed (Fig. 3.7) [22].

The side view in the detailed Fig. 3.6B is depicting the incoming laser beam getting scattered by a RBC in the blood vessel. In this figure, β is the angle between the blood flow velocity $\vec{v}_{RBC}$ and the x-y-plane. β can also be described as the angle that the blood flow velocity $\vec{v}_{RBC}$ is tilted with respect to the plane spanned by the two detection direction vectors. If the blood vessel follows a straight line it can be incorporated as a factor of $cos\beta$ into the calculation of the velocity of the RBCs, v_{RBC}. Often though the measurement device or the sample is tilted in a way, that $\beta = 0$ and consequently the factor $cos\beta = 1$. However, in the general case v_{RBC} can be written as [31, 32]

$$v_{RBC} = \frac{\Delta f_{max} \cdot \lambda_0}{n_b \cdot |cos(\delta)| \cdot cos(\beta)}. \tag{3.28}$$

The absolute velocity of the RBCs in the blood vessel can be determined using Eq. (3.28) for both detectors (both detectors are installed in the x-y-plane and have the same β)

$$v_{RBC} = \frac{\Delta f_{max1} \cdot \lambda_0}{n_b \cdot |cos(\delta_1)| \cdot cos(\beta)} = \frac{\Delta f_{max2} \cdot \lambda_0}{n_b \cdot |cos(\delta_2)| \cdot cos(\beta)}. \tag{3.29}$$

Another representation of Eq. (3.29) is

$$\Delta f_{max1} = \frac{v_{RBC} \cdot n_b \cdot |cos(\delta_1)| \cdot cos(\beta)}{\lambda_0}$$
$$\Delta f_{max2} = \frac{v_{RBC} \cdot n_b \cdot |cos(\delta_2)| \cdot cos(\beta)}{\lambda_0}. \tag{3.30}$$

Subtracting both equations leads to

$$\Delta f_{max1} - \Delta f_{max2} = \frac{v_{RBC} \cdot n_b \cdot cos(\beta)}{\lambda_0} \cdot \left[|cos(\delta_1)| - |cos(\delta_2)|\right], \qquad (3.31)$$

and with both Doppler angles in the same quadrant $(90° < \delta_1, \delta_2 < 180°)$,

$$\Delta f_{max1} - \Delta f_{max2} = \frac{v_{RBC} \cdot n_b \cdot cos(\beta)}{\lambda_0} \cdot \left[cos(\delta_1) - cos(\delta_2)\right]. \qquad (3.32)$$

The idea is now to get the velocity only as a function of the two frequency differences $\Delta f_{max1}, \Delta f_{max2}$ that are measured and the angle difference $\Delta\alpha$ between the two detectors. For that reason, we take a closer look at the cosine functions:

$$\begin{aligned}
cos(\delta_1) - cos(\delta_2) &= cos(90° + \gamma + \alpha_1) - cos(90° + \gamma + \alpha_2) \\
&= cos(90°) \cdot cos(\gamma + \alpha_1) - sin(90°) \cdot sin(\gamma + \alpha_1) \\
&\quad - cos(90°) \cdot cos(\gamma + \alpha_2) + sin(90°) \cdot sin(\gamma + \alpha_2) \\
&= -sin(\gamma + \alpha_1) + sin(\gamma + \alpha_2). \qquad (3.33)
\end{aligned}$$

The angles α_1, α_2 and γ are small (Fig. 3.7) and therefore, the arguments of the sinus functions $(\gamma + \alpha_1)$ and $(\gamma + \alpha_2)$ are small as well. With $sin(x) \approx x$ for small angles Eq. (3.33) can be written as

$$cos(\delta_1) - cos(\delta_2) = -(\gamma + \alpha_1) + (\gamma + \alpha_2) = \alpha_2 - \alpha_1 = \Delta\alpha. \qquad (3.34)$$

The maximum angle difference $\Delta\alpha$ between the two detectors can not exceed the maximum entrance angle of the rat eye. As discussed in Chap. 2, the maximum entrance angle and therefore, the maximum angle difference between the two detectors is $\Delta\alpha \sim 11°$.
Entering Eq. (3.34) into Eq. (3.32) leaves

$$\Delta f_{max1} - \Delta f_{max2} = \frac{v_{RBC} \cdot n_b \cdot cos(\beta)}{\lambda_0} \cdot \Delta\alpha. \qquad (3.35)$$

Rewriting Eq. (3.35) leads to the absolute velocity of RBCs in a blood vessel

$$\boxed{v_{absRBC} = \frac{\lambda_0 \cdot \Delta^* f_{max}}{n_b \cdot \Delta\alpha \cdot cos(\beta)}} \quad , \qquad (3.36)$$

with $\Delta^* f_{max} = \Delta f_{max1} - \Delta f_{max2}$ and $\Delta\alpha$ enters in radiant [2, 33–35].

4. Measurement hardware and data acquisition program

The project is in cooperation with the Institute of Systems Engineering from the HES-SO Valais-Wallis in Sion, Switzerland, which provided the measurement system (hardware and DAQ program) that is used. The device was used there a while ago as a compact single detector Laser Doppler Flowmetry (LDF) system and data acquisition was done on an old computer with an out of date operating system from today's point of view. This single detector system is described in Chap. 4.1. As mentioned in Chap. 3.3.2, a single detector system is able to measure the relative blood flow velocity. Since the previously used computer for data acquisition and the operating system are outdated, the LDV data acquisition for this thesis is done on a new computer with a different peripheral component interconnect (PCI) card and therefore, the provided program must be reviewed and changes have to be done (Chap. 4.2). The following sections take a closer look at the provided hardware and DAQ program and changes to them are described.

4.1 Measurement hardware

4.1.1 Measurement system from HES-SO Valais-Wallis

A block diagram of the single detector measurement system provided from the HES-SO Valais-Wallis is depicted in Fig. 4.1. This block diagram is divided in four sub-blocks: the confocal LDF unit, the common unit, the illumination unit (with the eye in front as sample) and the imaging unit.

The confocal LDF unit includes a LD as light source (I_1) (780 nm, 5 mW, Thorlabs, Munich, Germany), a 50/50 beam splitter (BS_2), a lens (L_3) and an optical fiber (I_2) in a confocal arrangement. The unit includes the same components as a Michelson interferometer except for the reference mirror (see/compare Chap. 3.1.1).
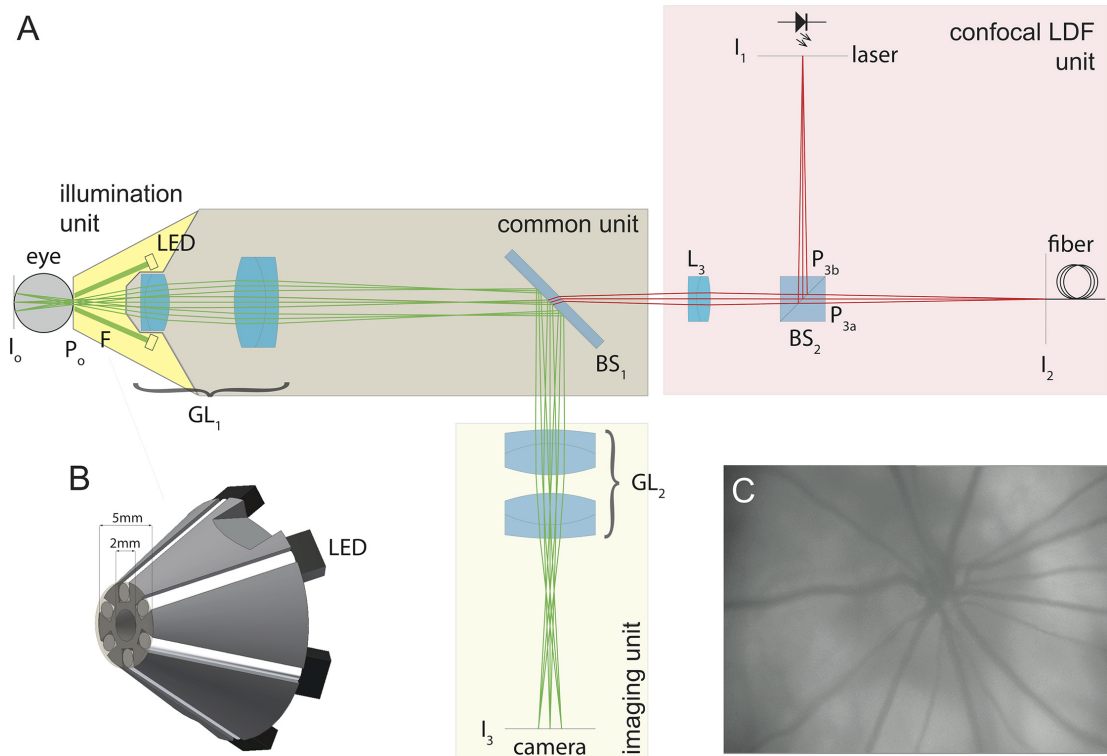
Figure 4.1: Single detector measurement system provided from the HES-SO Valais-Wallis (adapted from M. Mentek and F. Truffer [3] with permission from F. Truffer).

With an eye as sample and considering the principles of OMS, the setup should be usable for the measurement of the relative velocity of the RBCs in the blood flow in retinal blood vessels (see Chap. 3.3.1).

The laser light emitted from the LD I_1 gets deflected by the beam splitter BS_2, goes through the lens L_3, the common unit and the illumination unit and enters the rat's eye through the pupil P_0. The power level of the LD can be adjusted in three stages (300, 400 or 500 µW). All three power levels are delivering a light intensity into the rat eye that is below the minimum light intensity that would cause harmful effects to the photoreceptors of the rat [3, 36]. The light is scattered by the moving RBCs and the vessel wall of a blood vessel in the retina in I_0. The moving RBCs cause a Doppler shift to the laser light proportional to their speed. Some part of the scattered light is reflected back into the optical system, where the Doppler shifted part from the RBCs and the non-shifted part from the vessel wall get mixed. The collected mixed infrared light passes the cold mirror BS_1 and the beam splitter BS_2 and is directed towards an optical fiber I_2. Connected to the back of the optical fiber I_2, an APD (C5460-01, Hamamatsu, Japan) is used as detector that measures the beating frequency or frequency difference between the Doppler shifted light backscattered by RBCs and the non-shifted light backscattered by the blood vessel wall (see Chap. 3.3.2).

The common unit   receives the focused light from the lens L_3 of the confocal LDF unit. The cold mirror BS_1 filters the incoming light and only lets the light near the infrared spectrum pass [37]. With the lens combination GL_1 the laser beam is focused onto the rat retina. The estimated focused spot diameter on the rat retina is ~ 10 µm. The backscattered near infrared light passes the cold mirror BS_1 back into the confocal LDF unit and is collected by the fiber I_2 (200 µm diameter; Thorlabs, Munich, Germany). The fiber I_2 collects light around the focused spot with a diameter of ~ 80 µm.

The illumination unit   consists of six glass rods, each with a color filter (central wavelength, 530 nm; Edmund Optics, Karlsruhe, Germany) and a white light emitting diode (LED) (LW P4SG-U2AA-5K8L-Z, Osram, Munich, Germany) glued to the back. The front ends of the glass rods are arranged in a circle around the exit point of the laser light coming from the LD. Together the LEDs deliver up to 830 µW power of light into the eye and illuminate the fundus with green light in the visible range. The illumination with green light provides the highest contrast between the vessels and the surrounding tissue. The green light has no effect on the measurement signal (near infrared light) reaching the fiber I_2, because it is deflected by the cold mirror BS_1 and reaches the imaging unit.

The imaging unit   is basically a lens pair GL_2, which focuses the light coming from the common unit onto a charge-coupled device (CCD) camera with 640x480 active pixels (20K13XUSB, Videology, The Netherlands). The CCD camera allows visualisation of the retina and the projection of the laser onto the target via a software on the computer screen (Fig. 4.1 C).

4.1.2   Assembled box for power supply and PC connection from HES-SO Valais-Wallis

Additionally to the single detector measurement system, there is an assembled box from HES-SO Valais-Wallis, which is the measurement system's power supply and includes all hardware to set the right hardware settings (Fig. 4.2). Furthermore, the box serves as connection from the measurement system to the PCI card in the computer (also called data acquisition (DAQ) card). The PCI card (NI PCIe6251) enables data acquisition with the provided program.

The front side of the box (Fig.4.2 A) can be divided into three parts. The first part (Fig.4.2 A,1) includes the hardware used to control the LD. On the very left a turn-switch is integrated to select the three available power levels, Min $\hat{=}$ 300 µW, Med $\hat{=}$ 400 µW and Max $\hat{=}$ 500 µW (see also the paragraph on the confocal unit in Chap. 4.1.1). Next to it is a toggle switch, responsible for switching on the
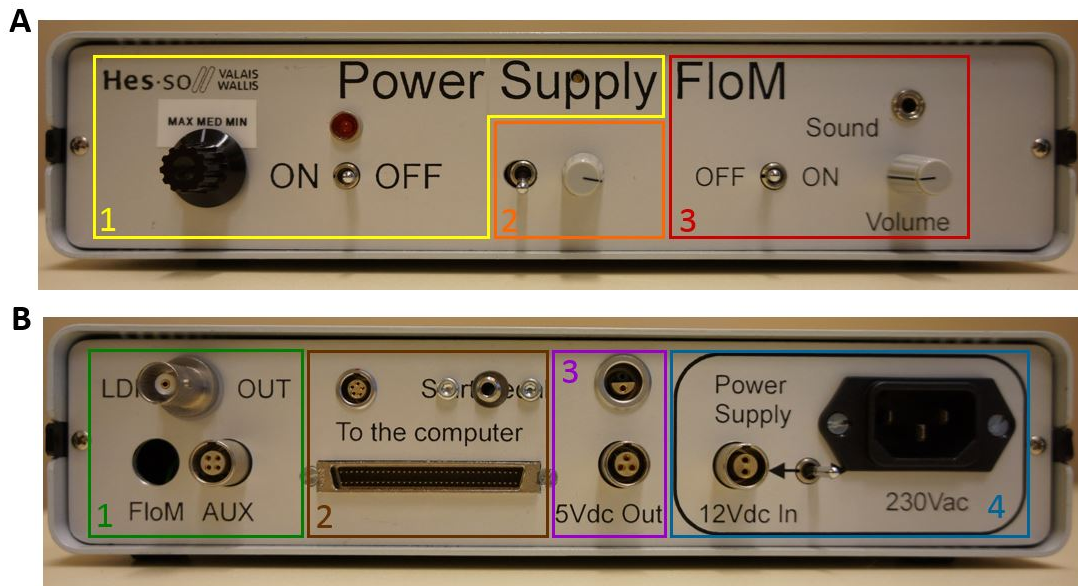
Figure 4.2: A) Front side and B) back side of the assembled box provided from the HES-SO Valais-Wallis, connecting the measurement system with the PC. All hardware settings have to be set on that box.

LD. If the LD is switched on, the red LED above lights up. On the upper side in the middle there is a little screw sunk into the cover, which is responsible for the amplification of the LD signal. For security reasons the amplification is turned down to a minimum while transportation and has to be turned up before use. It is placed behind the cover, in order to have it not accessible and turned by accident.

Beneath the screw is the second part (Fig.4.2 A,2). A second toggle switch is responsible for turning on the six LEDs from the illumination unit at the same time. It is not always necessary or even practical to have the probe site illuminated with all the available power of 830 μW, therefore, the knob on the right hand side can be used to adjust the brightness of the LEDs of the illumination unit (see also the paragraph on the illumination unit in the previous Chap. 4.1.1).

The third part is on the right side of the front cover (Fig.4.2 A,3). It includes a third toggle switch, which turns on a speaker installed inside the box. The beating frequency or frequency difference between the Doppler shifted light backscattered by RBCs and the non-shifted light backscattered by the blood vessel wall are within the acoustic frequency range and therefore, can be made hearable via the speaker. This helps with the adjustment of the laser beam. Since it is not always welcome to sound it out loud, there is a phone jack for a 3 mm plug built-in. The knob beneath the phone jack is used to turn up and down the volume of the sound signal.

The back side of the box (Fig.4.2 B) can be divided into four parts. The first part on the back side consists of two electrical connectors for audio signals (they were not used during experiments) (Fig.4.2 B,1).

The most important part is the second part on the right side next the audio signal connectors (Fig.4.2 B,2). On the bottom is the 68-pin electrical connector which builds the connection from the hardware box to the PCI card in the computer. On the left side above the electrical connector is the 5-pin power supply of the single detector measurement system, which supplies the LD and the CCD camera. Looking to the right, there is the input for the optical fiber leading to the APD used to collect the laser light signal (see the paragraph on the confocal unit in the previous Chap. 4.1.1).

The two electrical connectors on the right hand side are the third part (Fig.4.2 B,3). They were also not used during experiments and will not be described.

The fourth and last part is the main power supply of the box itself (Fig.4.2 B,4). It consists of a toggle switch in between two electrical connectors. With switching the toggle switch, the power input can be chosen to be $12Vdc$ or $230Vac$.

4.2   Data acquisition program

The DAQ program provided from HES-SO Valais-Wallis is a LabVIEW program. A basic understanding of LabVIEW was a prerequisite for this thesis. National Instruments made a change in their structure of LabVIEW for DAQ from Traditional NI-DAQ (Legacy) to NI-DAQmx [38]. The provided program is written in an old LabVIEW version with the Traditional NI-DAQ drivers, which unfortunately do not work with the new PCI card (NI PCIe6251) [39]. Therefore, the provided program is not executable. The first step is to get an executable program, which is done by replacing several sub-VIs (virtual instrument (VI), small program parts gathered in a library that are ready for a fast use) in the background of the program from Traditional NI-DAQ to NI-DAQmx. This is done in LabVIEW 2013 in version 13.0. In the following, the first executable LabVIEW program version is described starting with the different screens and the background and then changes to it leading from a LDF to a LDV data acquisition program and to the final program version are explained in Chap. 4.2.3 and 4.2.4.

4.2.1   Screens of the program from HES-SO Valais-Wallis

Welcome screen of the program

The provided LabVIEW program is composed of five different screens. The first screen is a welcome screen with a friendly reminder, that the LD needs to be turned on at least 20 minutes before use.

With the "Exit"-button on the welcome-screen, the program can be immediately closed. After clicking the "Continue..."-button the program continues to the input

screen.

Input screen of the program

The input screen of the program is depicted in Fig. 4.3.
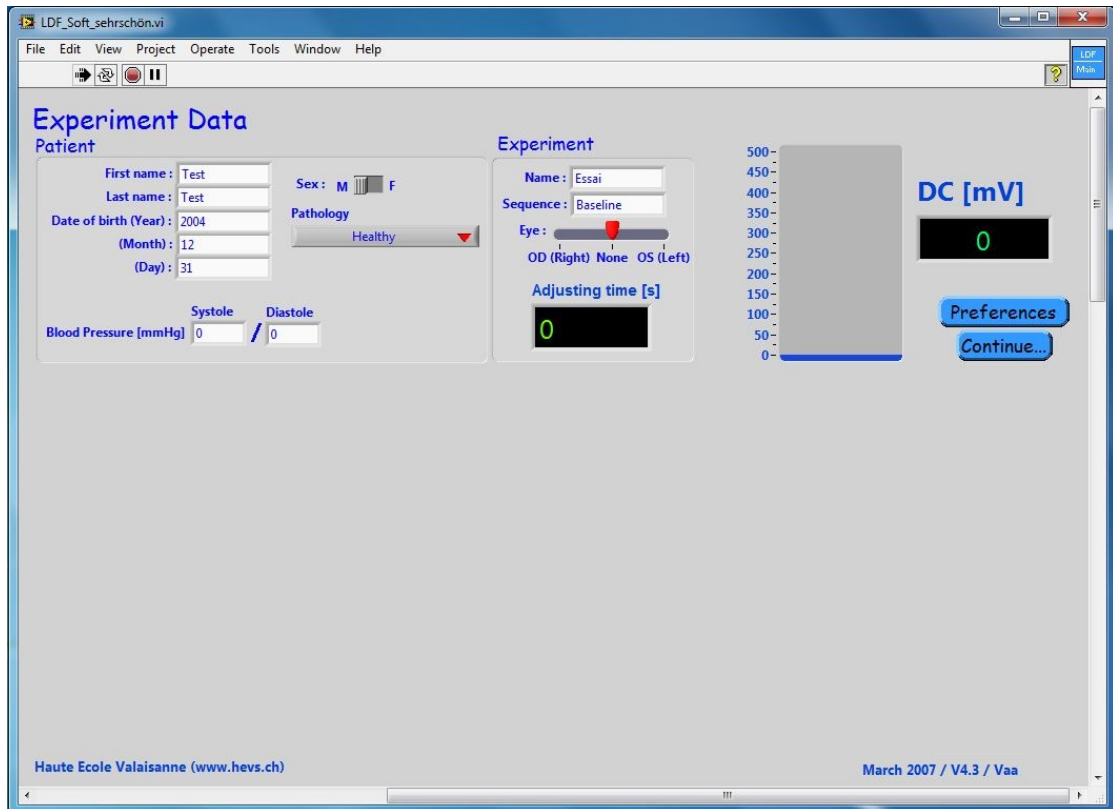
Figure 4.3: Input screen of the LabVIEW program.

Since the program was designed for measurements in human patients, the input screen provides input boxes for personal info of the patient (first name, last name, date of birth in year, month, day and sex), two input boxes for the systole and diastole value of the patients blood pressure and a drop down menu for medical input of the patients condition (called "pathology").

Furthermore, there is an input section for experiment data. One box is reserved for the experiments name and one is named "sequence". In this section there is also a toggle switch for choosing the measured eye ("OD Right" or "OS Left") and a display showing the adjusting time for each measurement, which is the timespan between leaving the input screen and starting a measurement. Without choosing the eye, the program can not be continued and an error message appears. This serves the user as a reminder to check if the correct eye is in front of the measurement device.

The level display on the right hand side, shows the direct current (DC) level in units of mV and is connected to the value display next to it. The intensity measured by the detector corresponds to the DC value. With the DC level the stability of the scattered light and therefore, the eye can be estimated [3]. When the "Preferences"-button on the input screen is clicked, a screen pops up, on which additional inputs for the measurements can be set. With clicking the "Continue..."-button the program switches to the measurement screen.

Preferences screen of the program
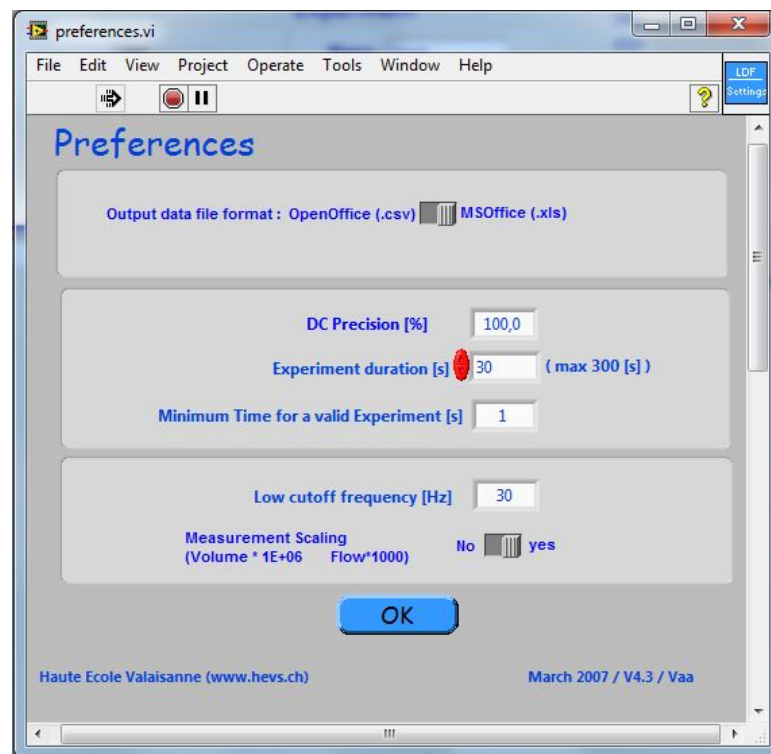
Figure 4.4: Preferences screen of the LabVIEW program.

The first additional input on the preferences screen is a toggle switch, that enables the choice of the data type ending between Open Office (".csv") and MS Office (".xls") (Fig. 4.4). The next input choice affects the "DC precision", which can be chosen in percent. It filters data points with improbable DC changes from sudden loss of intensity, which are caused by eye movements (see also Chap. 4.2.1). In the control below, the measurement time can be set. A measurement has a minimum time length of 1 second and can be stretched up to 300 seconds. The second input box sets the minimum time span for a valid measurement. A measurement counts as valid, if the DC precision is achieved for the time span set in the third input box. During a measurement, slow movements of the rat (or the patient) can occur due to breathing. Therefore, a frequency high-pass is included in the program, that filters

these movements, which have small velocities (typical value is 30Hz). Another input box is reserved for the low cutoff frequency of this frequency high-pass. The toggle switch below that input box is used to switch on a scaling factor for the measured volume and blood flow, which is useful for LDF, but not needed for LDV. With clicking the "OK"-button, the preference screen is closed.

Measurement screen of the program

The settings on the preferences screen usually stay the same for a series of measurements. After they are set, the patients data and condition are put in, the experiment name is set and the eye is chosen, it can be continued from the input screen onto the measurement screen. The measurement screen of the program is just an addition to the input screen. As soon as the "Continue..."-button on the input screen is clicked, all program elements except the DC display of the input screen are disabled and the program elements used for a measurement are made visible (Fig. 4.5).

Figure 4.5: Measurement screen of the program with the visible program elements used for a measurement after clicking the "Continue..."-button on the input screen.

The white, blank text-input can be used to leave comments. The pathology drop-down menu on the input screen has an "other" choice as last option. The idea for

that choice is, that an unusual condition can be described in the comments text-input on the measurement screen. With the "START"-button below the comments text-input, the measurement can be started. During the measurement the pulse can be monitored via the display "Pulse/min". On the right hand side another display, that lies between two adjustable values with red arrow buttons, shows the current DC value. With the red arrow buttons of the adjustable values, the level borders of the long DC display to the right can be changed. The borders should be shifted in a range around the DC value (displayed in the middle). If the borders are well chosen, the long DC display shows the development of the DC value over time, starting at 0 seconds till the end of the measurement (DC value and intensity are correlated, see "Input screen of the program" above). The end of the measurement is previously set with the control of the measurement time span on the preferences screen (see the paragraph "Preferences screen of the program"). This measurement time span is now shown on the measurement screen in the display called "View [s]". The measurement can be stopped any time with the "OPERATOR STOP"-button beneath the "START"-button. During each measurement, a display pops up that shows the current status.

Underneath the status display are two more displays. The first one shows the folder name, in which all files gathered during one measurement are saved. The folder name is assembled from the measurement date, the starting time of the measurement, two letters of the patients first name and last name and the chosen eye. The second display shows the actual date and time. After each measurement, the intra ocular pressure (IOP) can be measured and put into the provided input box in units of mmHg. On the right hand side there is a display titled "Measurement time [s]" showing the passed time span of the measurement in seconds. Above this display is a label, assessing if the measurement is valid or not. Beneath the long DC display, next to the measurement time display and the validation label is a big, black display which is empty as long as the measurement is running. As soon as the measurement is done, this display shows a summary of the results and the "Close the measurement"-button is enabled. With the "Close the measurement"-button, the measurement can be closed and the end screen opens.

End screen of the program

The end screen of the program assures that the measurement data is saved and offers the option for a new data acquisition. With the "Exit"-button on the end screen, the program can be closed. The "New acquisition"-button restarts the program and leads directly to the input screen (see the paragraph "Input screen of the program" in Chap. 4.2.1).

4.2.2 LabVIEW background of the data acquisition program

The background of the provided DAQ program from HES-SO Valais-Wallis is a LabVIEW program on 15 levels of a "Stacked Sequence Structure". Before changes can be made, the use of each of the 15 levels has to be understood. While finding of each level of the program, the program elements on each level were arranged in a new, cleaner way. For a better overview over the program, short comments are given. The program background is depicted as a flow chart in Fig. 4.6.

In the following paragraphs a short description of all levels from 0 to 14 is given. This serves the purpose, that a possible successor can go through all levels and can understand the program and its functionality.

0. Level

On level zero two file paths are generated: First, the path where the application is installed and second, the path where the measured LDV data should be saved in. In the LDV-data path an extra folder "LDF" is generated, in which all measurements are saved.

1. Level

The first level can be split into two parts. The first part sets the program elements of the measurement screen of the program invisible. This is necessary, if more than one measurement in a row is done and the program is started repeatedly.

The second part enables the program elements of the input screen. It includes the input boxes of patients data, pathology and experiment parameters.

2. Level

The second level consists of two parts again. In the first part, the hardware of the computer is checked for a PCI card. If there is no PCI card installed, the program can't collect any data and is stopped.

In the second part the first items are connected to the measurement screen of the program. The string of the comments text-input and the result display are emptied, the measurement time span is set to zero and the data type ending is registered.

3. Level

The third level is a while loop with two parts. The first part represents the background of the preferences screen. With a true/false query, the program settings are either taken from the previous measurement (case: False) or they are changed (case: True) on the preferences screen (see the paragraph "Preferences screen of the program" in 4.2.1).
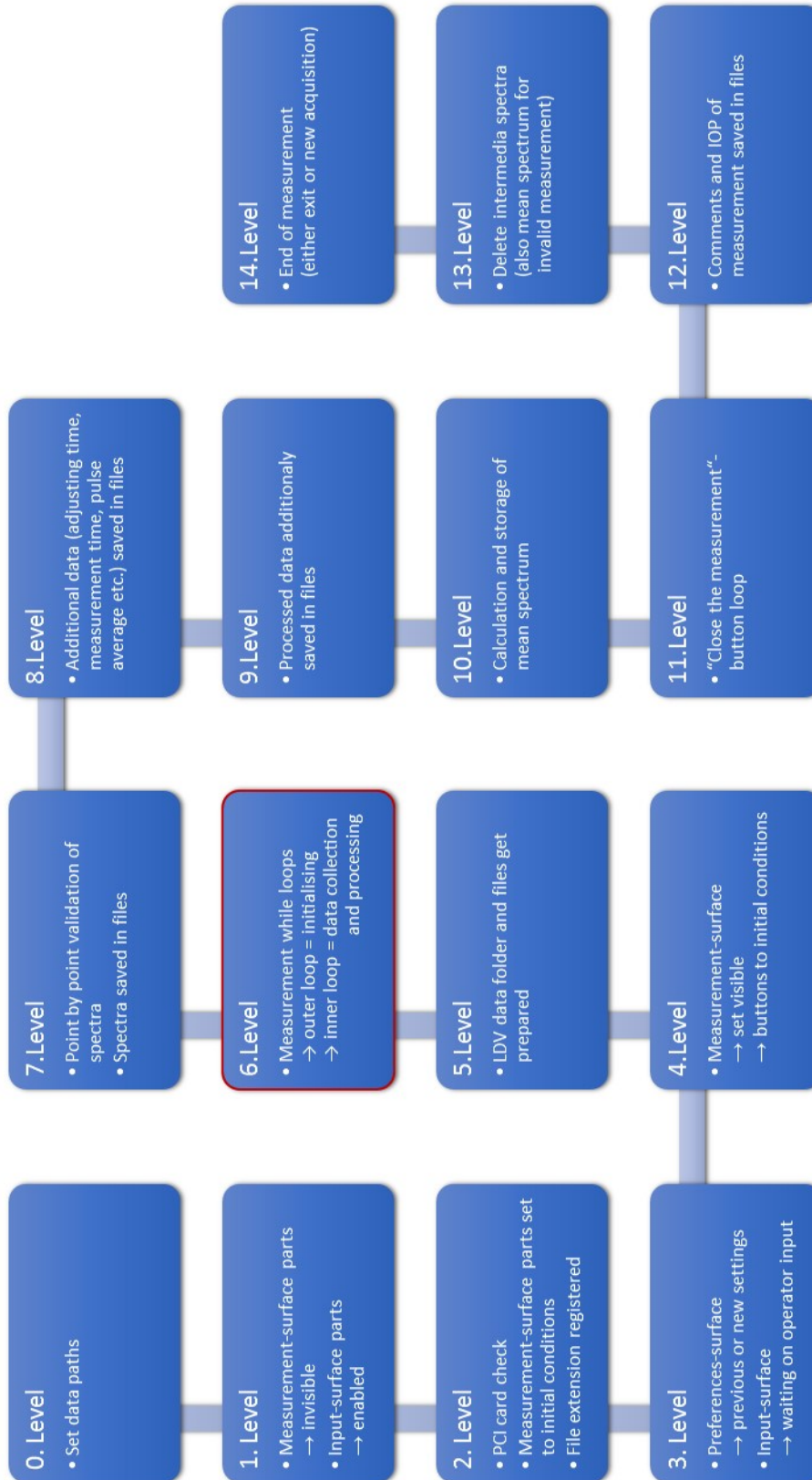
Figure 4.6: Flowchart of all 15 levels of the LabVIEW program used for data acquisition.

The second part is the while loop representing the background of the input screen of the program. The loop is waiting for the user to put in all the information about the patient: the first name, last name, date of birth, sex, values of systole and diastole, choose the pathology from the drop down menu and the eye that is measured. The measured eye has to be chosen, otherwise an error message appears (see the paragraph on the "Input screen of the program" in 4.2.1).

4. Level

On the fourth level of the program, elements for the measurement screen are made visible (in the second part of the fourth level). Additionally on this level, the initial status of the "START"-, "OPERATOR STOP"- and "Close the measurement"-button are set: the "START"-button is enabled and the other buttons are disabled (see "Measurement screen of the program" in 4.2.1).

5. Level

This level of the LabVIEW program consists of a big structure of strings. All the patients data and experiment input from the input screen, as well as the information about the patients pathology and the chosen eye are combined to create the strings for the different file paths for the folder and the files where the LDV measurement data is saved (see the paragraph on the "Input screen of the program" in 4.2.1).

6. Level

The sixth level is the core of the program, indicated by the red border around the 6.level rectangle on the flow chart (Fig. 4.6). Most of the necessary changes of the program are made on this level (see 4.2.4). It contains two nested while loops, in which the measurement takes place. The sub-VIs in the while loops are often connected to a program element on the measurement screen. Their functionality is discussed in the paragraph "Measurement screen of the program" in 4.2.1.
In the outer while loop, the initial conditions from the input screen are set with the sub-VI called "LDF Init Array". The connection to the PCI card is done via two sub-VIs. The first one, a self generated sub-VI called "AI config mx", is located in the outer while loop and configures which analogue input (AI) of the PCI card the measurement signal is coming from.
That analogue measurement signal is then read during the measurement with the "DAQmx"-VI (a standard VI of the NI-DAQmx driver package) located in the inner while loop. In the inner while loop, the measurement of one time step takes place and it is cycled till the measurement time is passed or the measurement is interrupted. During a measurement, the self generated "LDF History"-VI feeds the generated data to the long DC display of the measurement screen. The digital input for the pulse signal display is connected via the self generated "LDF Pulse"-VI. The "LDF

Time Date"-VI (also self generated) supplies the correlated display with the actual date and a digital clock signal, which enables the display to show the actual time. During a measurement, the self generated "LDF View"-VI delivers the DC value to its display. The same VI sends a summary of the results to the result display on the measurement screen after a measurement is finished. With the "LDF Scale"-VI the set measurement time span from the preferences screen is integrated into the background of the program. Furthermore, this VI deals with the change of the borders of the DC value display. The collected data from the "DAQmx"-VI is passed on to the "LDF Time Frequ"-VI, which is a VI, generated for further processing. This VI filters the collected data, generates the frequency spectrum and its noise signal and sorts the data into the measurement parameters (DC value, Noise, Volume, Flow etc.). The processed data is passed to the last sub-VI in the measurement loop, "LDF Save Spect". With this sub-VI the spectrum of each time step ($\sim$ 14 times per second) is translated into an array of number strings, that can be saved. The "DAQmx Clear Task"-VI in the outer while loop is a standard VI of the NI-DAQmx driver package. This VI clears all parameters that were reserved during the measurement.

7. Level

The prepared arrays of the spectra from the "LDF Save Spect"-VI are processed on the 7th level within two sub-levels. The first sub-level (level 0) is dedicated to validate each spectrum point by point. The second sub-level discards the invalid points and saves the spectra in the previous generated data files (see the paragraphs on "0. Level" and "5. Level").

8. Level

On level eight, additional data like the adjusting time, the measurement time and the pulse average are written into the previously generated data files.

9. Level

The parameters of the processed data are saved in the generated data files on the ninth level.

10. Level

If the measurement is valid (or the results are computed anyway), the mean spectrum from the measurement and an appropriate file are generated and saved on level 10.

11. Level

The while loop on the 11th level enables the "Close the measurement"-button of

the measurement screen as soon as the measurement is done.

12. Level

On level twelve, the comments from the comment text-input and the measured IOP are added to the data files.

13. Level

Level thirteen is already a preparation of the program for a new data acquisition. If the measurement is valid, the intermediate spectra are deleted before a new measurement is started. The mean spectrum is empty for invalid measurements and is in that case also deleted.

14. Level

The last level, level fourteen, is simply the background of the end screen of the program. It is just a while loop waiting for the user to click either the "Exit"- or the "New acquisition"-button on the end screen of the program (see the paragraph on the "End screen of the program" in 4.2.1).

4.2.3   Changes to the LabVIEW background of the program

For a functional DAQ program for LDV measurements, changes to the program background as well as to the different screens have to be done.
In LabVIEW, property nodes are used to set/change properties of program elements, for example program elements can be set visible/invisible or enabled/disabled. Levels 0-4 are unchanged, except that additional property nodes are integrated to set the new program elements of the screens visible/invisible or enabled/disabled with the other program elements belonging to the screen they are put on (see the changes to the screens in the next Chap. 4.2.4). The first major change is on the 5th level, where an additional file path is created. In the file "Cutoff_velocities" provided for each measurement, the recorded LDV data is saved.
As mentioned before, the most major changes in the program are made on the 6th level in the measurement while loop. Each second 14 spectra are recorded. A spectrum is different for each detected constellation of RBCs and there are constantly RBCs fluctuating out of and into the detected area of the blood vessel. Thus, the spectrum display would change 14 times per second and together with frequency fluctuation cause a quite noisy signal, when each single spectrum is displayed. Therefore, instead of displaying each single spectrum, an averaged spectrum over $\sim 1,5$ seconds is generated via a shift register averaging the data of 21 detected spectra. The averaging scales down the noise signal and stabilizes the displayed spectrum. With the added sub-VI "LDV_evaluation" all calculations regarding the

evaluation of the recorded LDV data are done. Another sub-VI added to the 6th level, called "LDV_save", is responsible for saving all recorded LDV data.

Levels 7 through 12 and level 14 are unchanged and only on level 13 a change is made. The new function of level 13 is that either all spectra are deleted or all of them are saved. The decision to save or delete all spectra is made by the user via a new button included on the input screen of the program (see 4.2.4).

4.2.4   Changed screens of the program

The welcome- , preference- and end screen stay unchanged, but a few things are added to the input- and measurement screen of the program.

Changed input screen of the program

The button "Keep Spectra?" added to the input screen offers the choice to save all spectra (~ 14 spectra/second) detected during a measurement (Fig. 4.7). The button was added to give the opportunity to print each spectrum in case it is needed for validation. Keeping all spectra uses a lot of data space on the hard drive and it can be enough to just save the average spectrum, which is done in all valid cases.

Furthermore, two drop down menus are added to the input screen. They became necessary with the driver package change from Traditional NI-DAQ (Legacy) to NI-DAQmx. The menus are used to choose the task that is done within the measurement loop and which AI of the PCI card is used to carry the measurement signal.

Changed measurement screen of the program

In a little change to the measurement screen, the status-display is removed (Fig. 4.8). If a LDV measurement is taking place, the "Measurement time [s]" display is showing the progress anyway.

More important changes are the two added long displays showing the average velocity of the collected velocities (taken from the original LDF evaluation) and the averaged spectrum consisting of 21 detected spectra (see previous paragraph). Additionally, in this display several other graphs are included that show the results during a measurement. The x- and y-axis of the spectrum display can be changed by simply changing the numbers at the ends of the axis. Furthermore, to enable a scan through the spectrum in smaller frequency intervals, the x-axis is equipped with a scroll bar beneath. There are two controls to set some needed values during a measurement, for example the Doppler angle (the other one will be explained in Chap. 6). The arrows on the side enable the stepwise change. Next to those
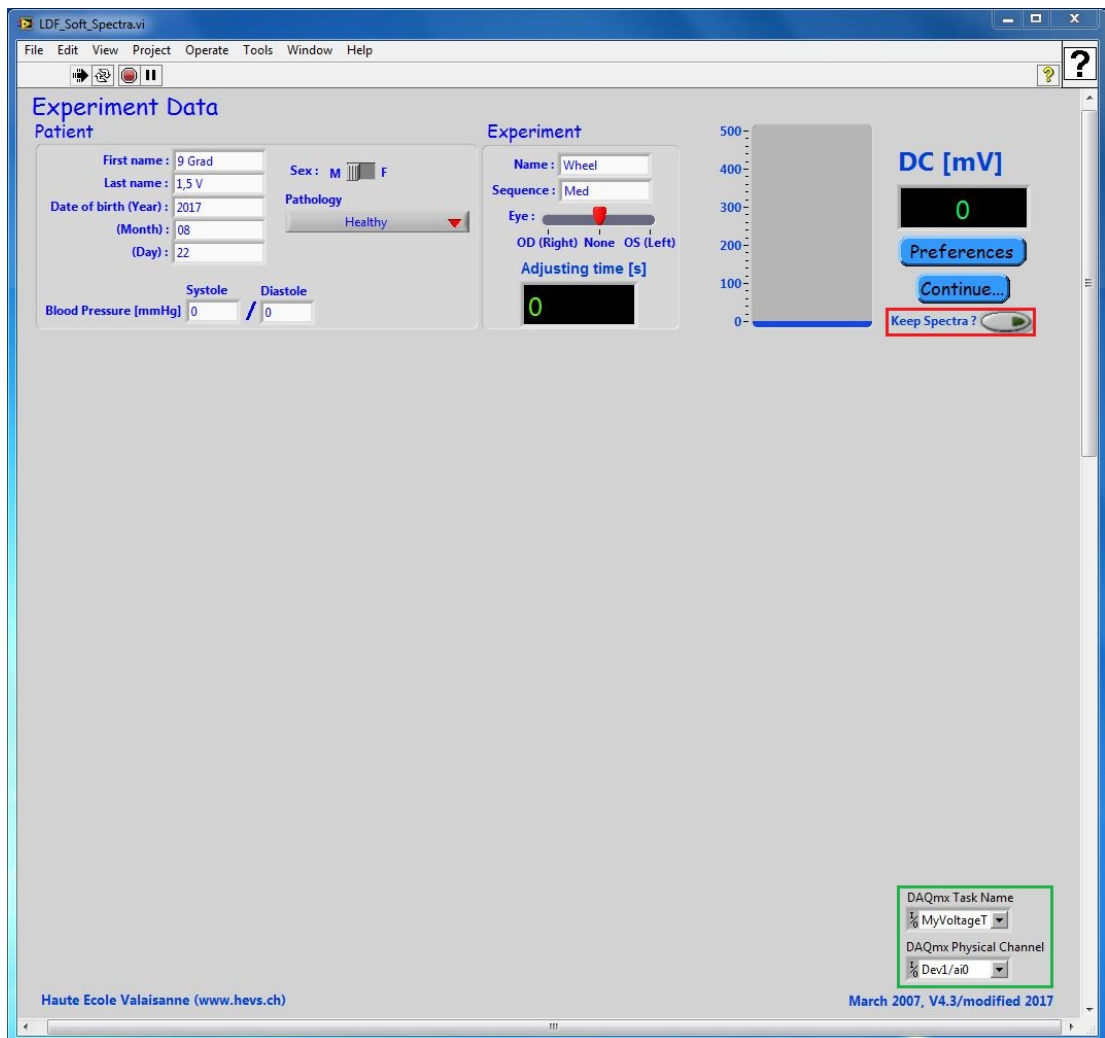
Figure 4.7: Changed input screen of the LabVIEW program. Two things are added: the "Keep Spectra?"-button, which enables the user to save all detected spectra during a measurement (red rectangle); via the drop down menus, the task within the measurement loop and the analogue input that carries the measurement signal are chosen (green rectangle).

controls seven indicators are given. They show the calculated results derived from
the averaged spectrum during a measurement. The indicators are arranged in two
columns, one for each experimental setup that is used for system validation and
program reliability (see Chap. 5).

Figure 4.8: Changed measurement screen of the LabVIEW program. The second display shows
the development of the average velocity (green rectangle) and the third display shows the averaged
spectrum during a measurement (orange rectangle). Also included in the third display are several
graphs for results derived from the averaged spectrum. The two controls are needed as additional
input during measurements (red rectangle). The two columns of three and four indicators are for
results of the different experimental setups (violet and blue rectangle). They are further described
in Chap. 6.

5. Measurement setups for in vitro system validation and program reliability

Two measurement setups are used to validate the single detector system with the changed DAQ program for LDV measurements. On both setups, a defined velocity can be set from which the expected frequency difference can be calculated and then the calculated frequency difference can be compared to the measured frequency difference for validation of the measurement.

5.1 Setup with rotating disc

In the first measurement setup, a rotating disc is used as a sample, because it is easy to use. The rotating velocity can be calculated and with an even surface, a clear angle between the incident laser beam and the surface plane can be set (Fig. 5.2). The velocity of the rotating disc is regulated via an electric motor which is connected to a power supply. The rotating disc together with the electric motor are mounted on a rotary table which can be used to set an angle between the incident laser beam and the surface plane of the disc, i.e. the Doppler angle.

The first step is to find the connection between the supplied voltage and the velocity of the rotating disc. The tangential velocity $\vec{v}$ of a rotating disc is calculated via the angular velocity $\vec{\omega}$ of the disc and the radius $\vec{r}$ (from the center to the measurement point, Fig. 5.1) with

$$\vec{v}_{tan} = \vec{\omega} \times \vec{r}. \tag{5.1}$$

Since the angular velocity and the radius are perpendicular to each other, the absolute value of the tangential velocity v_{tan} is the result of the product of the absolute values of the angular velocity ω and the radius r

$$v_{tan} = \omega \cdot r. \tag{5.2}$$
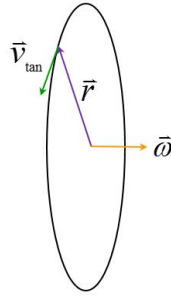
Figure 5.1: General picture of a rotating disc with radius $\vec{r}$ and angular velocity $\vec{\omega}$ for the calculation of $\vec{v}_{tan}$.

Generally, the absolute value of the angular velocity ω of a rotor is calculated with

$$\omega = 2\pi \cdot D, \tag{5.3}$$

where D is the number of rotations per seconds. Consequently, the absolute value of the tangential velocity v_{tan} can be determined with measuring two things: the radius r from the center to the measurement point on the rotating disc and the number of rotations per second D of the rotating disc with different voltages supplied to the electro motor

$$v_{tan} = 2\pi \cdot D \cdot r. \tag{5.4}$$

The disc consists of PTFE (also known as Teflon) and has a paper cover glued on top. The paper cover has a disconnected circular grid imprinted that is used as a guideline to always set the laser beam on the same position with the same radius r before beginning of the measurement. The used radius is $r = 16.1$ mm (Fig. 5.2).
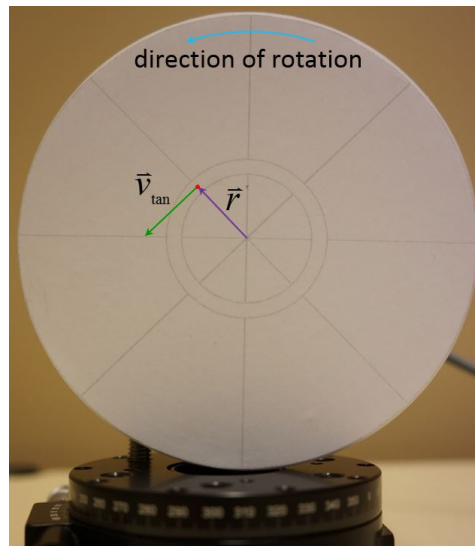
Figure 5.2: Rotating disc with the imprinted paper cover. The chosen radius $r = 16.1$ mm marks the measurement point where the incident laser beam hits the disc.

The measurement of the rotations per second with different supplied voltages leads to a characteristic curve for the used electric motor. The easiest way to get the characteristic curve is by stopping the time t and waiting for a certain amount of rotations S of the disc for several supplied voltages and then dividing the two values

$$D = \frac{S}{t}. \tag{5.5}$$

The absolute value of the tangential velocity v_{tan} can then be determined with

$$v_{tan} = \frac{2\pi \cdot S \cdot r}{t}. \tag{5.6}$$

In Tab. 5.1 the measured values of the characteristic curve of the used electric motor and the absolute value of the tangential velocity calculated with Eq. (5.6) and a radius of $r = 16.1$ mm are listed.

Table 5.1: Measured values of the characteristic curve of the used electric motor.

U (V)	S (Rotations)	t (s)	v_{tan} (mm/s)
0.5	10	360	2.81
0.8	10	188	5.38
1	10	164	6.17
1.2	10	129	7.84
1.5	10	108	9.37
1.7	10	90	11.24
2	10	76	13.31
2.2	10	68	14.88
2.5	10	60	16.86
2.7	10	55	18.39
3	10	47	21.52

The characteristic curve of the used electric motor is depicted in Fig. 5.3 (blue curve) and a linear approximation of the curve is included (red dotted line).

Since the characteristic curve of the electric motor is linear in the velocity interval relevant for RBCs in retinal vessels (3 - 16 mm/s, see Chap. 2), the linear slope $k_v \approx 7.2275 \frac{mm}{Vs}$ and the axis intercept $d_v \approx -0.9341 \frac{mm}{s}$ of the linear approximation can be used for further calculation [19]. Therefore, the absolute value of the tangential velocity of the rotating disc can be directly calculated from the set voltage with

$$\boxed{v_{tan} \approx k_v \cdot U + d_v}. \tag{5.7}$$

A top view of the setup consisting of the rotating disc mounted on the rotor of the electric motor and the single detector measurement system in front of it is depicted in Fig. 5.4 (compare to Fig.3.6).
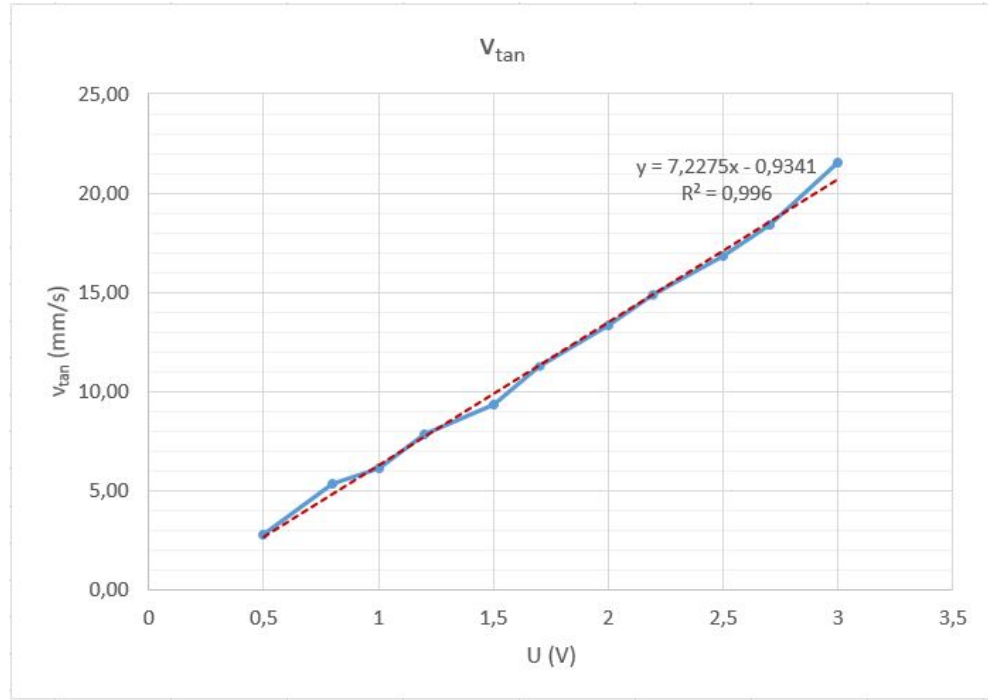
Figure 5.3: Characteristic curve between the rotations per second and the absolute value of the tangential velocity of the used electric motor (blue curve). Linear approximation of the characteristic curve (red dotted line).

Considering the theoretical derivation made in Chap. 3.3.2, the absolute value of the tangential velocity of the rotating disc from Eq. (5.7) simulates the velocity of the RBCs from Eq. (3.27)

$$v_{RBC} = v_{tan}$$
$$\frac{\Delta f_{max} \cdot \lambda_0}{n_b \cdot |cos(\delta)|} = k_v \cdot U + d_v \ . \tag{5.8}$$

The paper cover of the rotating disc demands the use of the refractive index of paper $n_p = 1.56$ instead of the refractive index of blood n_b [40].
The maximum frequency difference generated by the rotating disc can be calculated with

$$\boxed{\Delta f_{max} = \frac{n_p \cdot (k_v \cdot U + d_v)}{\lambda_0} \cdot |cos(\delta)|} \ . \tag{5.9}$$

All variables in Eq. (5.9) except the voltage of the power supply of the electric motor and the Doppler angle are now determined. The electric motor together with the rotating disc is mounted on a rotary table that is able to set a defined Doppler angle δ between the incident laser beam and the surface plane of the rotating disc. To verify the functionality of the hardware and the DAQ program of the single detector system, the setup is used by setting a certain voltage to supply the electric motor
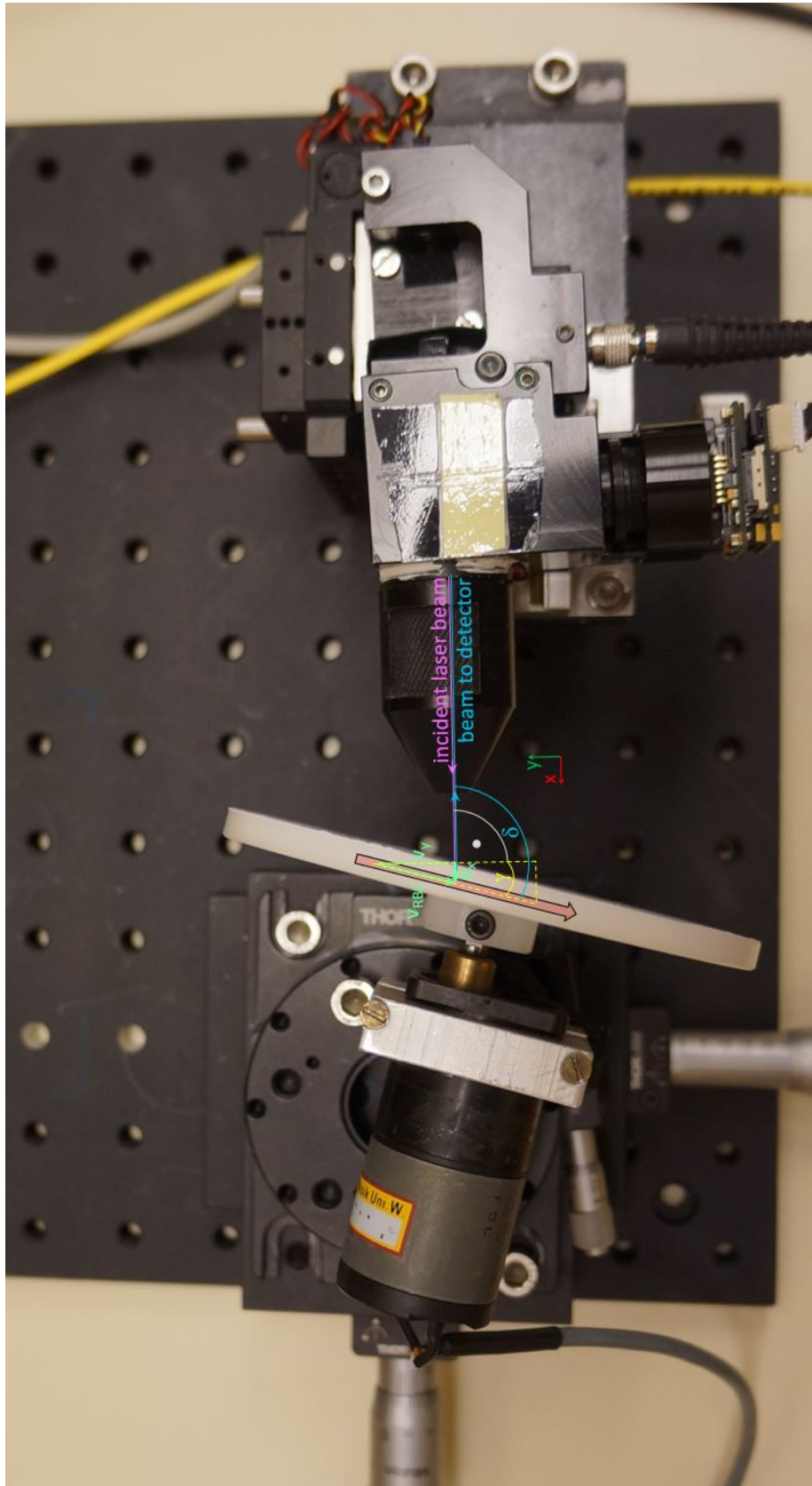
Figure 5.4: Measurement setup with rotating disc and single detector measurement system for in vitro system validation.

and measuring the frequency difference Δf_{max} generated by the rotating disc at several Doppler angles.

5.2   Setup with capillary

The second in vitro measurement setup is already near to an in vivo experiment. A syringe pump simulates the function of the heart and pumps blood through a glass capillary that simulates a blood vessel and serves as sample. The capillary is mounted on a rotary table which can be used to set an angle between the incident laser beam and the direction of the blood velocity flowing through the capillary. In a first step the connection between the supplied flow rate of the syringe pump and the blood velocity in the capillary has to be found. The mean blood velocity in a capillary v_{mean} can be calculated with the equation for the mean velocity in a pipe

$$v_{mean} = \frac{Q_{cap}}{A_{cap}}, \tag{5.10}$$

where Q_{cap} is the flow through the capillary in mm$^3/s$ and A_{cap} is the capillaries cross section in mm^2. The syringe pump delivers the supplied flow in units of ml/h. To get the flow in mm$^3/s$ a factor of 3.6 needs to be integrated in the equation

$$v_{mean} = \frac{Q_{cap}}{3.6 \cdot A_{cap}}, \tag{5.11}$$

where Q_{cap} now has to be inserted in ml/h. The maximum velocity of fluid flow in a capillary is in the middle of the cross section. With the assumption of a parabolic velocity profile in the capillary, the mean velocity is half of the maximum velocity v_{max} in the center of the capillary $v_{mean} = \frac{v_{max}}{2}$ ([2], p.133). Taking into account that blood is a non-Newtonian fluid, the conversion factor between maximum and mean velocity lies between 1.6 and 1.8 and thus [41]

$$v_{mean} \approx \frac{v_{max}}{1.8}. \tag{5.12}$$

Consequently Eq. (5.11) can be written as

$$v_{max} = \frac{Q_{cap} \cdot 1.8}{3.6 \cdot A_{cap}} = \frac{Q_{cap}}{2 \cdot A_{cap}}. \tag{5.13}$$

The cross section of a capillary (or pipe) matches the area of a circle and is calculated with

$$A_{cap} = \frac{d_{cap}^2 \cdot \pi}{4} \tag{5.14}$$

Inserting Eq. (5.14) into Eq. (5.13) leads to

$$v_{max} = \boxed{\frac{Q_{cap} \cdot 4}{2 \cdot d_{cap}^2 \cdot \pi} = \frac{2 \cdot Q_{cap}}{d_{cap}^2 \cdot \pi}} \, . \tag{5.15}$$

A top view of the setup consisting of the glass capillary and the single detector measurement system in front of it is depicted in Fig. 5.5 (compare to Fig.3.6).

Considering the theoretical derivation made in Chap. 3.3.2, the maximum blood velocity v_{max} from Eq. (5.15) matches the velocity of the RBCs v_{RBC} from Eq. (3.27).

$$v_{RBC} = v_{max}$$
$$\frac{\Delta f_{max} \cdot \lambda_0}{n_b \cdot |cos(\delta)|} = \frac{2 \cdot Q_{cap}}{d_{cap}^2 \cdot \pi} \tag{5.16}$$

The refractive index of whole human blood can be calculated with Cauchy's formula at the wavelength of the used LD of $\lambda_0 = 780nm$ (see Chap. 4.1.1) with [42]

$$n_b = 1.357 + \frac{6.9 \cdot 10^3}{\lambda_0^2} + \frac{7.6 \cdot 10^8}{\lambda_0^4} \approx 1.37 \quad (\lambda_0 \text{ in nm}) \, . \tag{5.17}$$

The diameter of the capillary is determined with an optical coherence tomography (OCT) measurement. The OCT has a image depth of 4096 pixels which corresponds to 1.98 mm in air. The capillary takes 609 pixels. The diameter of the capillary can be calculated with

$$d_{cap} = \frac{609}{4096} \cdot 1.98 \approx 0.2944 \text{ mm} \tag{5.18}$$

Thus, the diameter of the capillary $d_{cap} \sim 294.4$ µm is larger than a the diameter of a blood vessel in the rat eye $(4.4 - 50$ µm, see Chap. 2) [20, 21].
The maximum frequency difference generated by the RBCs in the capillary can be calculated with

$$\Delta f_{max} = \boxed{\frac{2 \cdot n_b \cdot Q_{cap}}{\lambda_0 \cdot d_{cap}^2 \cdot \pi} \cdot |cos(\delta)|} \, . \tag{5.19}$$

All variables of Eq. (5.19) except the flow rate of the syringe pump and the Doppler angle are now determined. The capillary is mounted on a rotary table that is able to set a defined Doppler angle δ between the incident laser beam and the velocity of the RBCs in the bloodstream. To verify the functionality of the hardware and the DAQ program of the single detector system, the setup is used by setting a certain flow rate on the syringe pump and measuring the frequency difference Δf_{max} generated by the moving RBCs in the capillary at several Doppler angles.
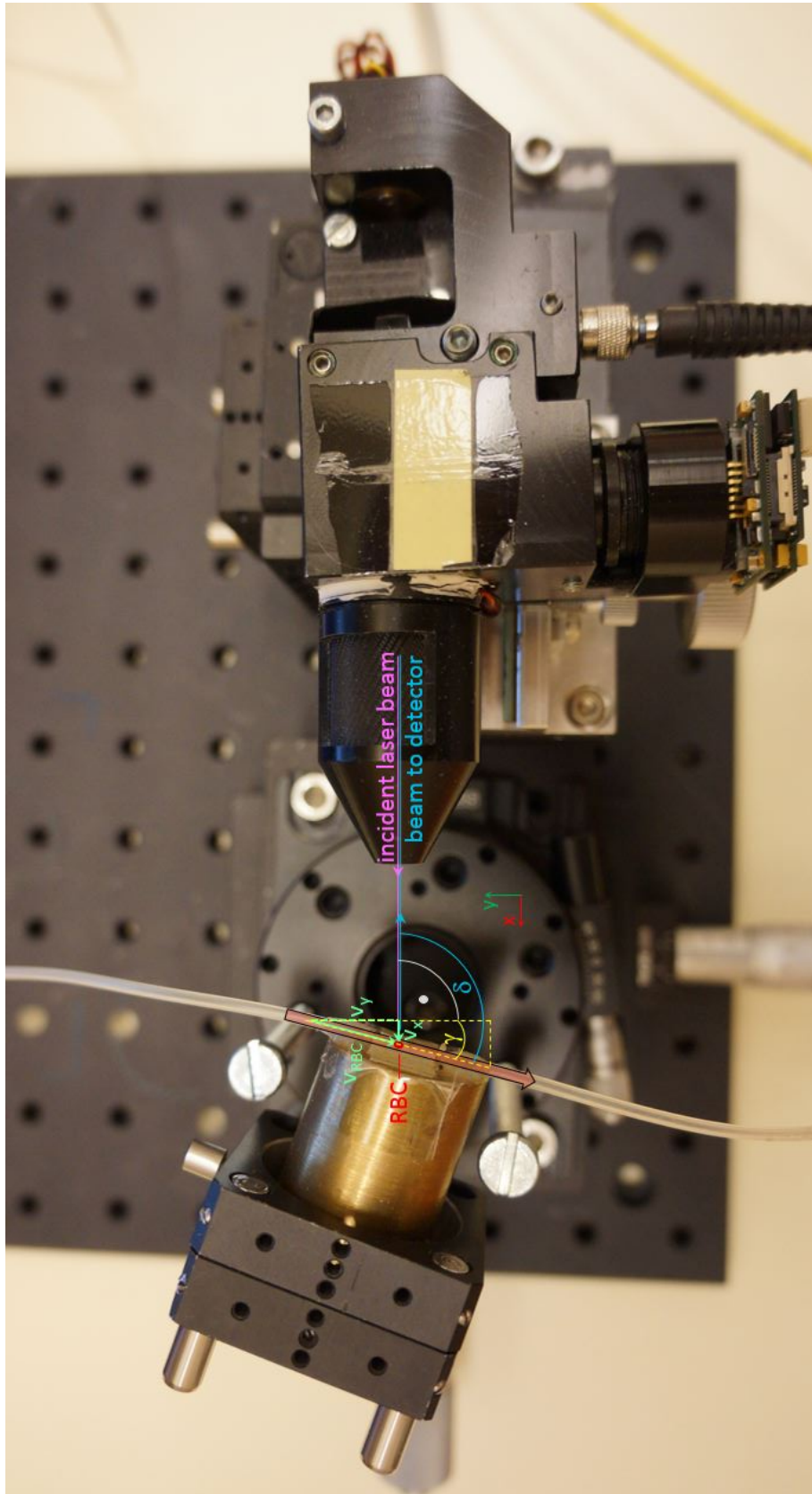
Figure 5.5: Measurement setup with glass capillary and single detector measurement system for in vitro system validation.

6. Measurement results

6.1 Results for setup with rotating disc

The power supply of the electric motor is set to a fixed voltage of $U = 1.5$ V which is equivalent to a fixed velocity of the rotating disc of $v_{tan} = 9.91$ mm/s. This velocity lies in the middle of the velocity interval relevant for RBCs in retinal vessels ($3 - 16$ mm/s, see Chap. 2) [19]. The refractive index of paper $n_p = 1.56$, the linear slope $k_v \approx 7.2275 \frac{mm}{Vs}$ and the axis intercept $d_v \approx -0.9341 \frac{mm}{s}$ of the linear approximation (see Chap. 5.1) and the wavelength of the used LD $\lambda_0 = 780$ nm $= 780 \cdot 10^{-6}$ mm (see Chap. 4.1.1) are inserted into Eq. (5.9) [40]

$$
\begin{aligned}
\Delta f_{max} &= \frac{n_p \cdot (k_v \cdot U + d_v)}{\lambda_0} \cdot |cos(\delta)| \\
&= \frac{1.56 \cdot (7.2275 \cdot 1.5 - 0.9341)}{780 \cdot 10^{-6}} \cdot |cos(\delta)| \\
&= 19814.3 \cdot |cos(\delta)| \, .
\end{aligned}
\tag{6.1}
$$

After inserting all mentioned parameters, the frequency difference Δf_{max} in Eq. (6.1) is only a function of the Doppler angle δ. With the rotary table, a defined Doppler angle δ between the incident laser beam and the surface plane of the rotating disc can be set. To validate the single detector system and the changed DAQ program, the frequency difference Δf_{max} is measured for different Doppler angles δ.

A measurement result is generated by switching on the power supply (set to $U = 1.5V$), setting a Doppler angle and taking a measurement for $30s$. An exemplary screenshot of the changed DAQ program's measurement screen made during a measurement is depicted in Fig. 6.1.

For these measurements, the input boxes in the input screen part are used to identify the measurement folder: first name is the set Doppler angle, last name is the set power supply voltage, the experiments name is "Wheel" and in the sequence is the used power level of the LD. The long DC display in the measurement screen part shows a little unsteady intensity level. That pulsation originates from the motor axis that does not run perfectly smooth and the glue, which is not perfectly even
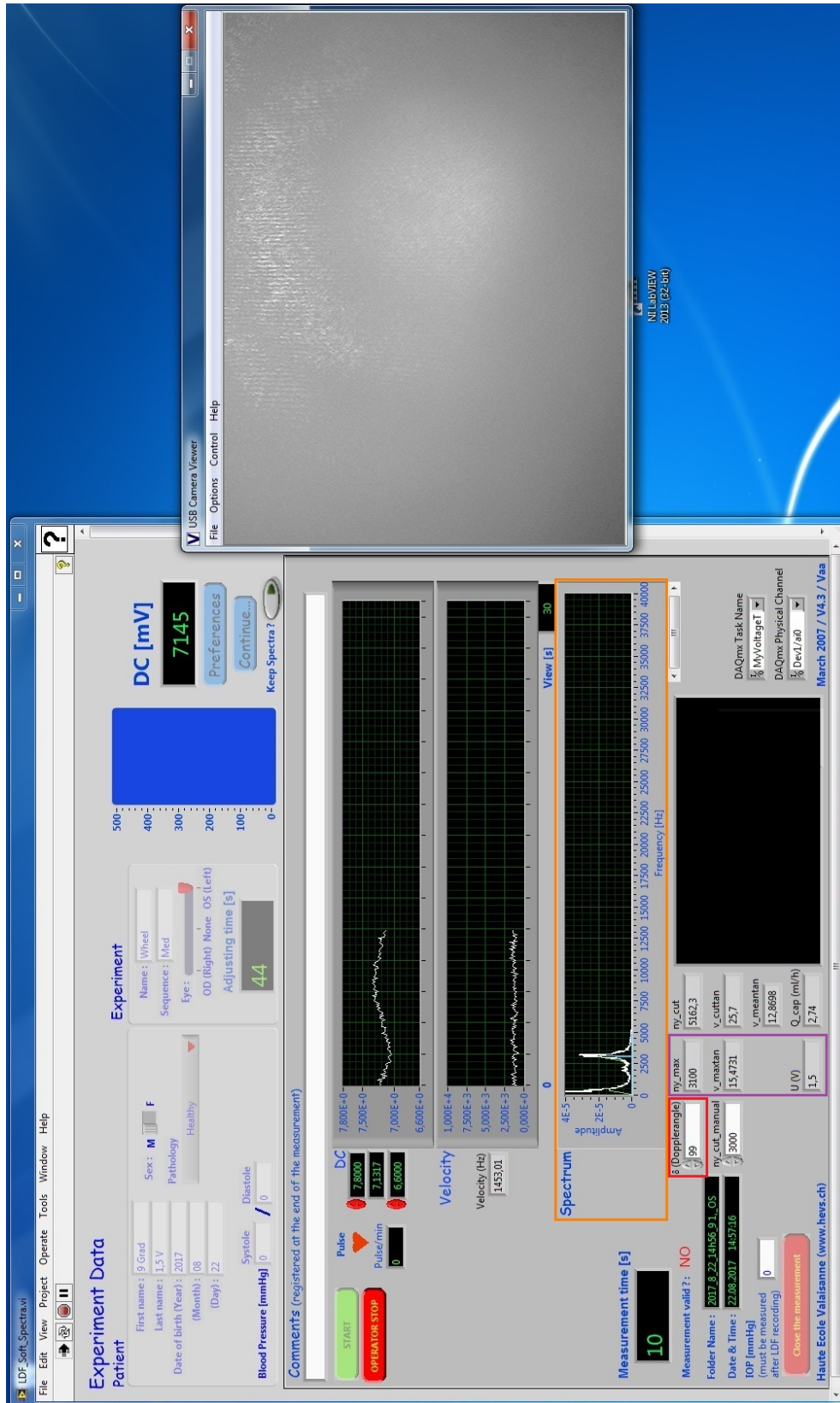
Figure 6.1: Screenshot made during a measurement with the rotating disc setup. On the left, the measurement screen of the changed DAQ program and on the right, the screen of the software showing the video made with the CCD camera are depicted. The coloured frames highlight the most important parts of the measurement screen: the orange frame is surrounding the spectrum display, the red frame highlights the input boxes and the purple frame highlights the indicators relevant for measurements with the rotating disc setup.

distributed between the paper cover and the surface of the disc. Nevertheless, the long "Velocity" display, showing the time course of the average velocity, indicates that a steady average velocity is measured. The averaged power spectrum shown in the third long display has one distinct peak that represents the measured frequency difference. The spectrum generated by the measurement of the frequency difference of the rotating disc is not flat up to a cut-off frequency as the predicted power spectrum of the LDV theory (Fig. 3.5), because the rotating disc yields another velocity profile. As depicted in Fig. 5.2, the measurement point is far from the center of the rotating disc. Thus, the rotating disc setup gives a velocity profile in an interval of velocities around the measurement point that does not start at zero and corresponds to a frequency interval or spectral width of the signal (see Chap. 3.3.2). As mentioned in Chap. 4.2.4, there are additional graphs included in the spectrum display in Fig. 6.1. The peak of the frequency interval is automatically followed by the blue graph integrated into the programs spectrum display and taken as the measured frequency difference Δf_{max} (Fig. 6.1). Therefore, the smaller the spectral width of the signal, the more precise is the measurement. Via the first control beneath the spectrum display of the measurement screen, the Doppler angle is set and integrated into the DAQ program.

The first column of indicators next to the control displays the results during a measurement of the rotating disc setup. They display the currently measured frequency difference Δf_{max} in units of Hz (in "ny_max"), the measured velocity v_{tan} resulting from that frequency difference (in "v_maxtan") and, to make the evaluation of the result easy during measurements, the expected set voltage of the power supply of the electric motor calculated back from the measured frequency difference Δf_{max} (in "U(V)"). All calculations are done in the background in the "LDV evaluation" sub-VI (Chap. 4.2.3).

The LDV results are saved via the added sub-VI "LDV save" in the file "Cutoff_velocities" in the data folder prepared by the changed DAQ program's background (see Chap. 4.2.1). The "Cutoff_velocities" file includes the set Doppler angle δ, the time steps, the measured frequency difference Δf_{max}, the resulting velocity v_{tan} and the back calculated voltage U of the power supply for all time steps of the 30 seconds of the measurement. For each set Doppler angle, a result is created by averaging the measured frequency difference Δf_{max}, the resulting velocity v_{tan} and the back calculated voltage U over all time steps of the measurement. The averaged values are then manually put into a table and a graph depicting the frequency difference Δf_{max} as a function of the Doppler angle δ is generated. The quality of a measurement is evaluated with the mean absolute error (MAE) between the measured and the calculated graph.

To produce acceptable results with the rotating disc setup, several parameters have to be determined and set correctly. The measurement point needs to be set between the lines of the disconnected circular grid imprinted on the paper cover of the rotating disc. Furthermore, a measurement is getting more exact, the better the surface plane of the rotating disc is in the measurement system's point of focus. The point of focus of the measurement system is reached, when the spectral width is the

smallest and therefore, the peak in the power spectrum display of the measurement surface is most narrow. For this measurement setup, an exact determination of the linear approximation of the characteristic curve of the electric motor and therefore, the linear slope k_v and the axis intercept d_v are key. A measurement where the parameters of the linear approximation of the characteristic curve of the electric motor are not exactly determined is depicted in Fig. 6.2.

Figure 6.2: Frequency difference Δf_{max} as function of the set Doppler angle δ measured with the rotating disc setup. The measured frequency difference is the thick blue line, the calculated frequency difference is the red dotted line. The measured frequency difference is clearly increased over almost the whole measurement. The correlated MAE between the measured and the calculated graph over the entire function is ~ 483 Hz.

Another key parameter for a measurement is the determination in which position of the rotary table the Doppler angle δ is exactly 90°, i.e. the angle where no frequency shift is measured by the LDV system, because there is no component of $\vec{v}$ towards the measurement system. In case the determination is only a little bit off, the graph resulting from the measured frequency difference is shifted to the graph of the calculated frequency difference (Fig. 6.3).

Figure 6.3: Frequency difference Δf_{max} as function of the set Doppler angle δ measured with the rotating disc setup. The measured frequency difference is the thick blue line, the calculated frequency difference is the red dotted line. The measured frequency difference is slightly shifted to the left of the graph of the calculated frequency difference. The correlated MAE between the measured and the calculated graph over the entire function is ~ 154 Hz.

The values of a measurement result that was produced with the rotating disc setup are listed in Tab.6.1 and the correlated generated graph is depicted in Fig.6.4.

All three generated graphs (Fig. 6.2, 6.3, 6.4) show a clear correlation between the frequency difference Δf_{max} generated through the frequency shift caused by the velocity of the rotating disc and the absolute value of the cosine of the set Doppler angle δ as predicted by the theory (Eq. 3.25 and specific for this setup Eq. 5.9). Therefore, the single detector measurement system and the changed DAQ program seem to be applicable to make relative velocity LDV measurements and a further investigation with another setup is of interest.

Table 6.1: Measurement results for the rotating disc setup. δ is the set Doppler angle, Δf_{max} is the frequency difference, v_{tan} is the correlated velocity of the rotating disc and U is the voltage calculated from the frequency difference.

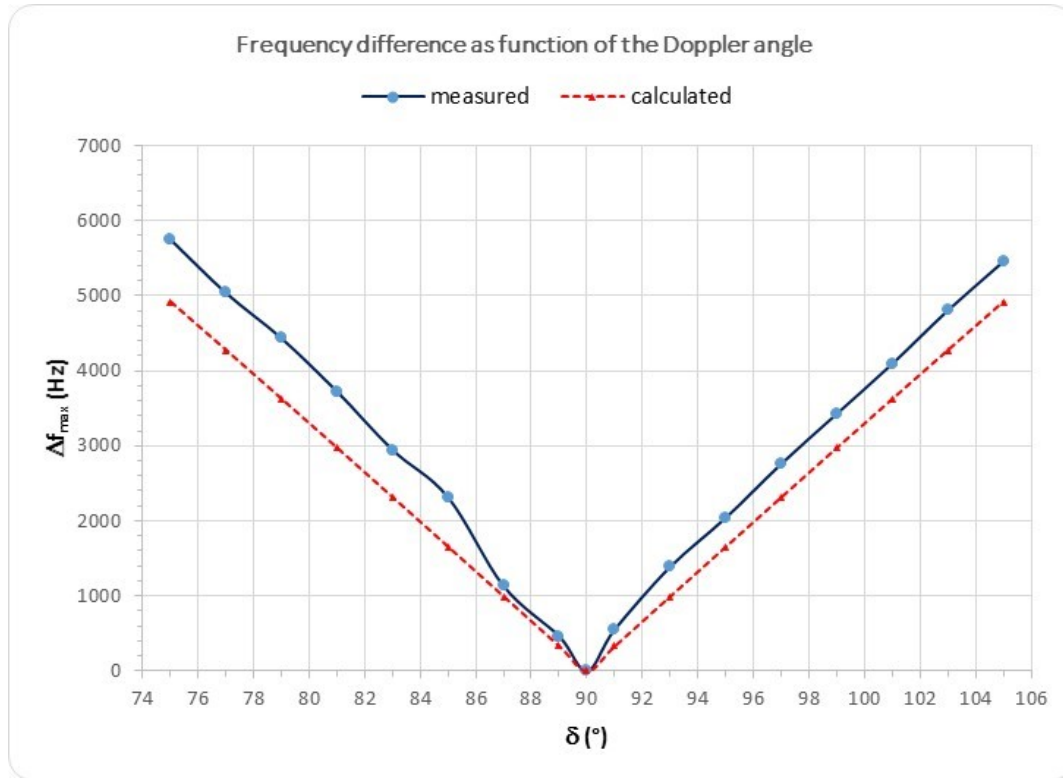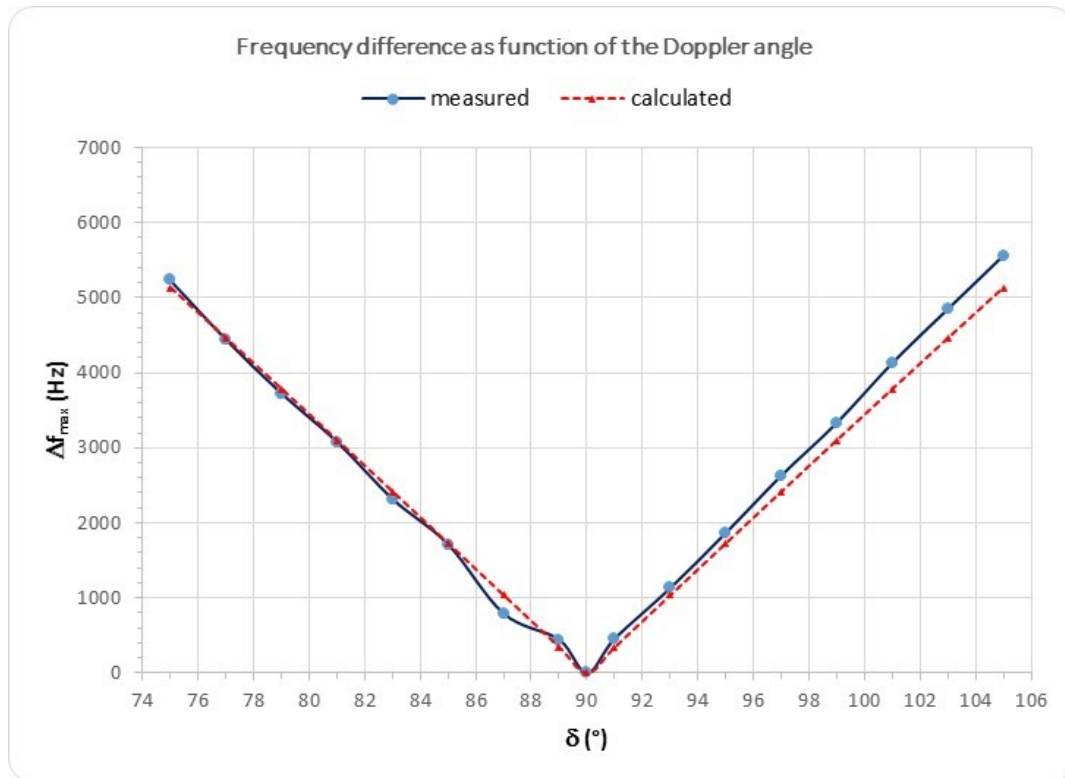| δ (°)	measured			calculated		
	Δf_{max} (Hz)	v_{tan} (mm/s)	U(V)	Δf_{max} (Hz)	v_{tan} (mm/s)	U(V)
75	5406.40	10.44	1.57	5128.32	9.91	1.5
77	4653.41	10.35	1.56	4457.25	9.91	1.5
79	4025.53	10.55	1.59	3780.75	9.91	1.5
81	3353.79	10.72	1.61	3099.64	9.91	1.5
83	2559.85	10.50	1.58	2414.76	9.91	1.5
85	1863.31	10.69	1.61	1726.93	9.91	1.5
87	1104.90	10.56	1.59	1037.00	9.91	1.5
89	463.37	13.28	1.97	345.81	9.91	1.5
90	0	0	1.50	0	9.91	1.5
91	449.03	12.87	1.91	345.81	9.91	1.5
93	879.51	8.40	1.29	1037.00	9.91	1.5
95	1617.49	9.28	1.41	1726.93	9.91	1.5
97	2361.53	9.69	1.47	2414.76	9.91	1.5
99	3125.31	9.99	1.51	3099.64	9.91	1.5
101	3824.16	10.02	1.52	3780.75	9.91	1.5
103	4555.57	10.13	1.53	4457.25	9.91	1.5
105	5257.19	10.15	1.53	5128.32	9.91	1.5
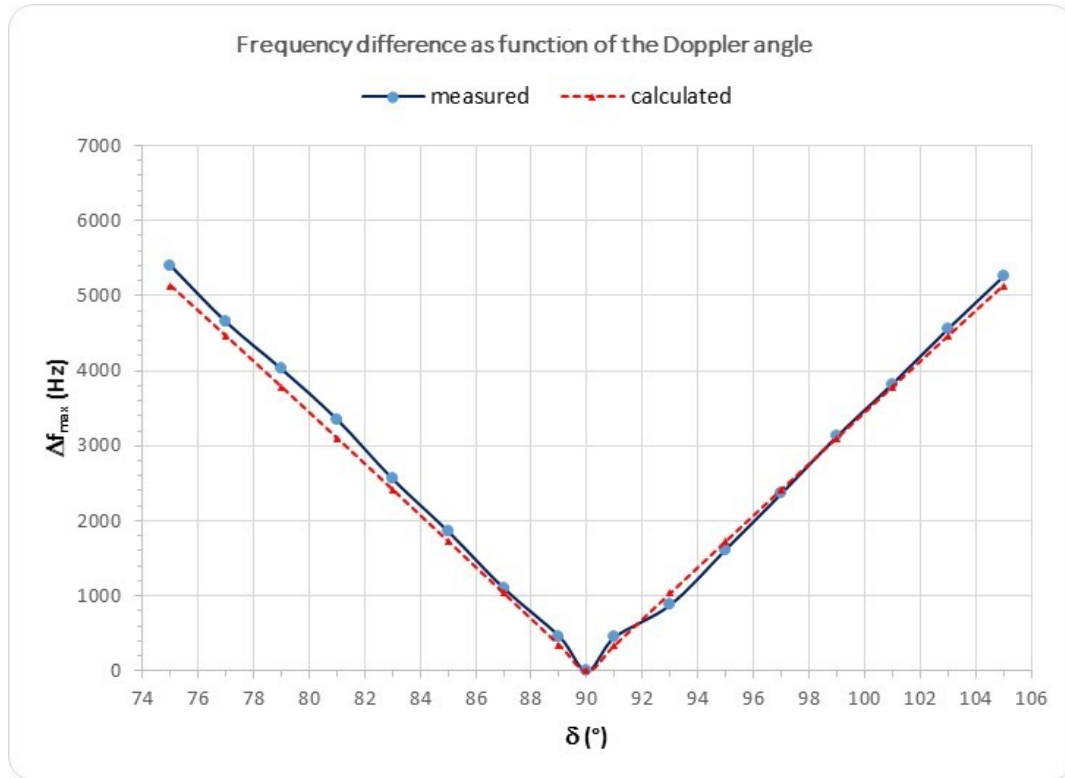
Figure 6.4: Frequency difference Δf_{max} as function of the set Doppler angle δ measured with the rotating disc setup. The measured frequency difference is the thick blue line, the calculated frequency difference is the red dotted line. The graph of the measured frequency difference is in good correlation with the graph of the calculated frequency difference. The correlated MAE between the measured and the calculated graph over the entire function is only ~ 127 Hz.

6.2   Results for setup with capillary

The flow rate of the syringe pump is set to a fixed value of $Q = 1.8$ ml/h which is equivalent to a maximum velocity of the RBCs in the bloodstream of $v_{RBC} = 13.22$ mm/s within the velocity interval relevant for RBCs in retinal vessels (3 - 16 mm/s, see Chap. 2) [19]. The refractive index of blood $n_b = 1.37$ at the used LDs wavelength Eq. (5.17), the diameter of the capillary Eq. (5.18) and the wavelength of the used LD $\lambda_0 = 780$ nm $= 780 \cdot 10^{-6}$ mm (see Chap. 4.1.1) are inserted into Eq. (5.19)

$$
\begin{aligned}
\Delta f_{max} &= \frac{1.37 \cdot 2 \cdot 1.8}{780 \cdot 10^{-6} \cdot 0.2944^2 \cdot \pi} \cdot |cos(\delta)| \\
&= 23223.8 \cdot |cos(\delta)| \, .
\end{aligned}
\tag{6.2}
$$

After inserting all mentioned parameters, the frequency difference Δf_{max} in Eq. (6.2) is only a function of the Doppler angle δ. With the rotary table, a defined Doppler

angle δ between the incident laser beam and the velocity of the RBCs in the blood-stream can be set. To validate the single detector system and the changed DAQ program, the frequency difference Δf_{max} for different Doppler angles δ is measured. An exemplary screenshot of the changed DAQ program's measurement screen made during such a measurement is depicted in Fig. 6.5.

For these measurements, the input boxes in the input screen part are used to identify the measurement folder: first name is the set Doppler angle, last name is the set flow rate of the syringe pump, the experiments name is "Capillary" and in the sequence is the used power level of the LD. The long DC display in the measurement screen part shows a steady intensity level and also the long "Velocity" display showing the progress of the average velocity indicates that a steady average velocity is measured. The averaged power spectrum shown in the third long display is flat up to a cut-off frequency as predicted by the theory (Fig. 3.5) and includes frequency differences correlated to a parabolic velocity profile with velocities starting at zero ($v = 0$) up to a maximum velocity ($v = v_{RBC}$). As mentioned in Chap. 4.2.4, there are additional graphs included in the spectrum display in Fig. 6.1. The maximum frequency difference Δf_{max} (cut-off) can be manually set via the second control beneath the spectrum and is integrated as a orange graph into the programs spectrum display (Fig. 6.5). Via the first control beneath the spectrum display, the Doppler angle is set and integrated into the DAQ program.
The second column of indicators next to the controls displays the results during a measurement of the capillary setup. They display the currently set maximum frequency difference Δf_{max} in units of Hz (in "ny_cut"), the measured velocity v_{RBC} resulting from that frequency difference (in "v_cuttan"), the mean velocity of the spectrum in units of mm/s (in "v_meantan") and, to make the evaluation of the result easy during measurements, the expected set flow rate of the syringe pump calculated back from the measured frequency difference Δf_{max} (in "Q_cap(ml/h)"). All calculations are done in the background in the "LDV evaluation" sub-VI (Chap. 4.2.3). The LDV results are saved via the added sub-VI "LDV save" in the file "Cut-off_velocities" in the data folder prepared by the changed DAQ program's background (see Chap. 4.2.1). The "Cutoff_velocities" file includes the set Doppler angle δ, the time steps, the measured frequency difference Δf_{max}, the resulting velocity v_{RBC} and the back calculated flow rate Q of the syringe pump for all time steps of the 30 seconds of the measurement. For each set Doppler angle a result is created by averaging the measured frequency difference Δf_{max}, the resulting velocity v_{RBC} and the back calculated flow rate Q over all time steps of the measurement. The averaged values are then manually put into a table and a graph depicting the frequency difference Δf_{max} as a function of the Doppler angle δ is generated. The quality of a measurement is evaluated with the MAE between the measured and the calculated graph.
To produce acceptable results with the capillary setup, several parameters have to be determined and set correctly. The measurement point needs to be set in the center of the capillary to make sure the maximum frequency difference Δf_{max} is
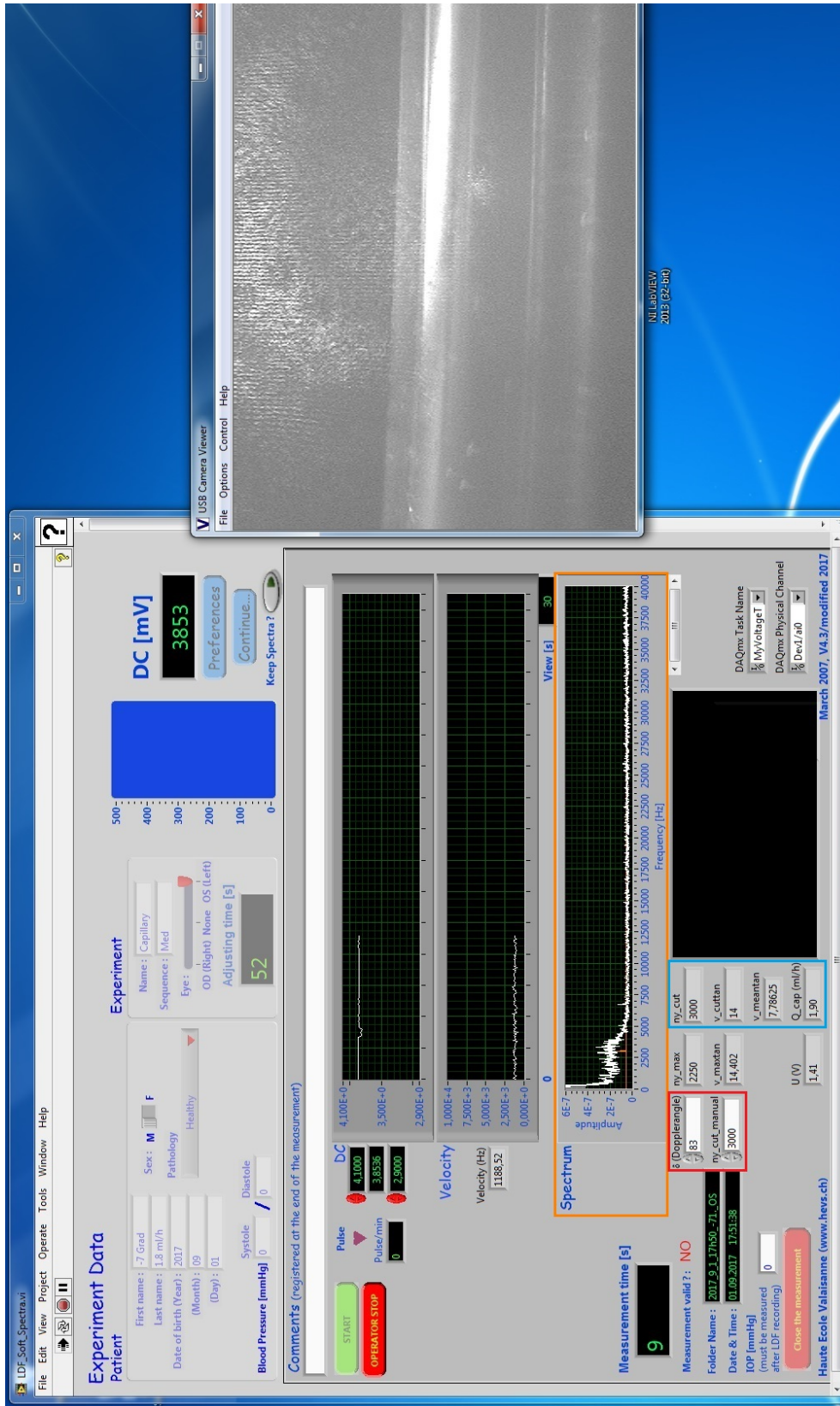
Figure 6.5: Screenshot made during a measurement with the capillary setup. On the left, the measurement screen of the changed DAQ program and on the right, the screen of the software showing the video made with the CCD camera are depicted. The coloured frames highlight the most important parts of the measurement screen: the orange frame is surrounding the spectrum display, the red frame highlights the input boxes and the light blue frame highlights the indicators relevant for measurements with the capillary setup.

measured. A measurement is only possible, if the capillary is in the measurement system's point of focus. The point of focus of the measurement system is reached, if the power spectrum has the characteristic shape of a parabolic velocity profile as discussed in Chap. 3.3.2 and depicted in (Fig. 3.5). Otherwise the power spectrum follows the shape of an exponential function. In Fig. 6.6 two exemplary spectra are depicted, one spectrum for a case where the capillary is out of focus and another spectrum where the capillary lies in the point of focus of the measurement system.
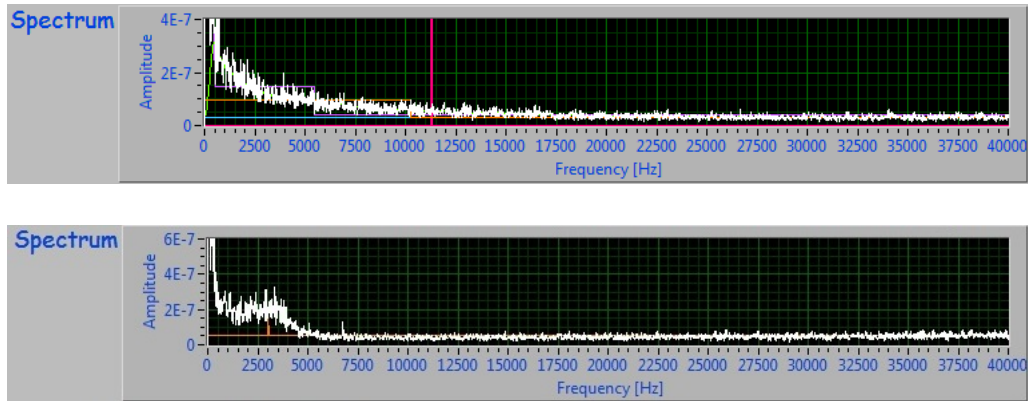
Figure 6.6: Spectra of different measurements. The first spectrum follows the shape of an exponential function and the cut-off frequency or maximum frequency difference Δf_{max} can not be determined (capillary not in focus). The second spectrum has a clear cut-off frequency (capillary in focus).

For this measurement setup, an exact determination of the capillary diameter is key. A measurement where the diameter of the capillary is not exactly determined is depicted in Fig. 6.7.

The values of a measurement result that was produced with the capillary setup are listed in Tab.6.2 and the correlated generated graph is depicted in Fig.6.8.

Both generated graphs (Fig. 6.7, 6.8) show a clear correlation between the frequency difference Δf_{max} generated through the frequency shift caused by the velocity of the RBCs and the absolute value of the cosine of the set Doppler angle δ as predicted by the theory (Eq. 3.25 and specific for this setup Eq. 5.19). Therefore, the single detector measurement system and the changed DAQ program is applicable to make relative velocity LDV measurements.

Figure 6.7: Frequency difference Δf_{max} as function of the set Doppler angle δ measured with the capillary setup. The measured frequency difference is the thick blue line, the calculated frequency difference is the red dotted line. The measured frequency difference is clearly increased over almost the whole measurement. The correlated MAE between the measured and the calculated graph over the entire function is ~ 740 Hz.

Table 6.2: Measurement results for the capillary setup. δ is the set Doppler angle, Δf_{max} is the measured frequency difference, v_{max} is the correlated velocity of the disc and U is the voltage calculated from the measured frequency difference.

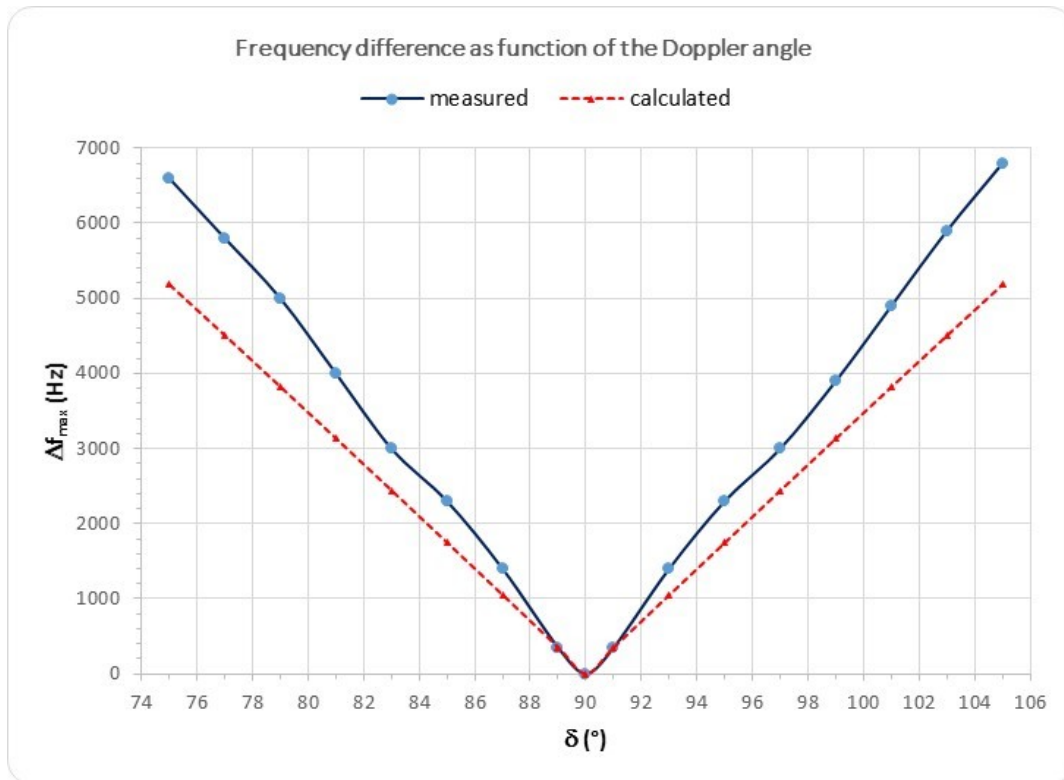|	measured			calculated		
δ (°)	Δf_{max} (Hz)	v_{max} (mm/s)	Q (ml/h)	Δf_{max} (Hz)	v_{max} (mm/s)	Q (ml/h)
75	6600	14.52	1.97	6010.77	13.22	1.8
77	5800	14.68	2.00	5224.22	13.22	1.8
79	5000	14.92	2.03	4431.31	13.22	1.8
81	4000	14.56	1.98	3633.00	13.22	1.8
83	3000	14.02	1.90	2830.27	13.22	1.8
85	2300	15.02	2.04	2024.09	13.22	1.8
87	1400	15.23	2.08	1215.44	13.22	1.8
89	350	11.42	1.55	405.31	13.22	1.8
90	0	0	0	0	0	1.8
91	350	11.42	1.55	405.31	13.22	1.8
93	1400	15.23	2.08	1215.44	13.22	1.8
95	2300	15.02	2.04	2024.09	13.22	1.8
97	3000	14.02	1.90	2830.27	13.22	1.8
99	3900	14.19	1.93	3633.00	13.22	1.8
101	4900	14.62	1.99	4431.31	13.22	1.8
103	5900	14.93	2.03	5224.22	13.22	1.8
105	6800	14.96	2.03	6010.77	13.22	1.8
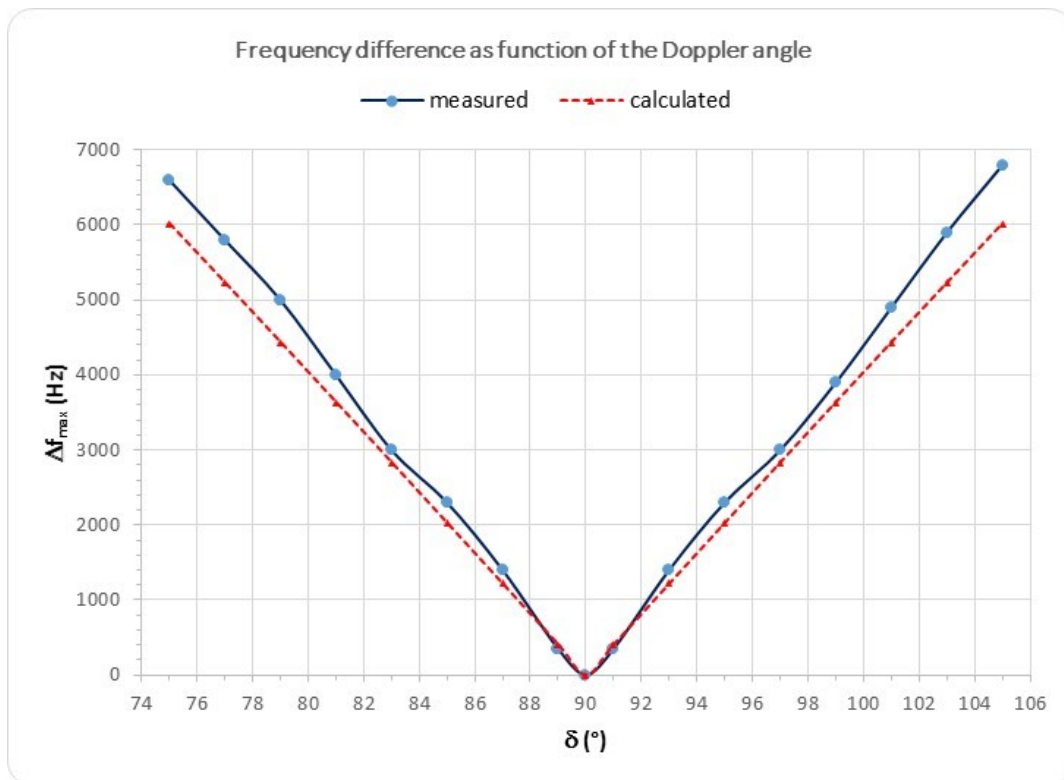
Figure 6.8: Frequency difference Δf_{max} as function of the set Doppler angle δ measured with the capillary setup. The measured frequency difference is the thick blue line, the calculated frequency difference is the red dotted line. The graph of the measured frequency difference is in good correlation with the graph of the calculated frequency difference. The correlated MAE between the measured and the calculated graph over the entire function is only ~ 334 Hz.

6.3   Result interpretation for measurement system with two detectors

From the results gathered with the capillary setup, a prediction for the most promising angle adjustment for a system with two detectors can be made. As calculated in Chap. 2, the maximum entrance angle into the rat's eye can be estimated with $\theta \sim 11°$. In Chap. 3.3.3 it was stated, that the maximum angle difference between the two detectors can not exceed this entrance angle and is $\Delta \alpha \sim 11°$.

Both maximum frequency differences Δf_{max1}, Δf_{max2} measured by the two detectors are absolute values and always positive. Since the absolute velocity of RBCs in a blood vessel is a function of $\Delta^* f_{max} = \Delta f_{max1} - \Delta f_{max2}$ (Eq. (3.36)), both angles α_1 and α_2 must be chosen in such a way that both measured maximum frequency differences are of the same sign. The safest way to guarantee such a system, is by setting up both detectors on the same side of the incident laser beam (Fig. 6.9).
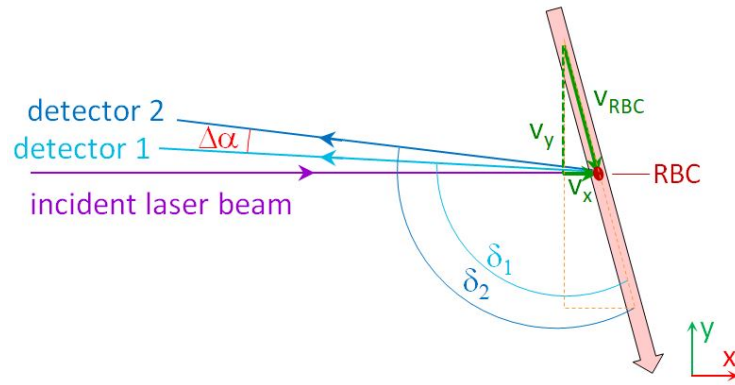
Figure 6.9: Measurement system with two detectors for measuring the absolute velocity of RBCs in a blood vessel.

Two measurement results for different Doppler angles made with the capillary setup can be used to calculate the angle difference $\Delta\alpha$ and with Eq. (3.36) the absolute velocity of RBCs v_{absRBC}. For the calculation it is assumed that the vector of the velocity direction is not tilted with respect to the detector plane and the angle $\beta = 0°$ (see detailed Fig. 3.6B). In Tab. 6.3 the results for all Doppler angle combinations are listed. Each column represents a fixed angle difference $\Delta\alpha$ between two Doppler angles (left column).

The measurements where done with a flow rate of $Q = 1.8$ ml/h which is equivalent to a maximum velocity of the RBCs in the bloodstream of $v_{RBC} = 13.22$ mm/s. Considering the theoretical value, the MAE between the measured absolute velocities v_{absRBC} and the theoretical absolute velocity v_{RBC} can be calculated. The results are listed in Tab. 6.4.

Looking at the MAE values in Tab. 6.4, the small MAE value is $-0.17 mm/s$ which relates to a relative measurement error of only $\sim 1.3\%$. This small MAE can be achieved with an angle difference $\Delta\alpha = 4°$ between two detectors at the Doppler angles $\delta_1 = 83°$, $\delta_2 = 87°$ or $\delta_1 = 93°$, $\delta_2 = 97°$ or $\delta_1 = 95°$, $\delta_2 = 99°$.

Table 6.3: From measurements calculated absolute velocity of RBCs for all combinations of Doppler angles. δ is the Doppler angle and $\Delta\alpha$ is the angle difference between the two detection directions.

δ (°)	v_{absRBC} (mm/s) at varible angle differences $\Delta\alpha$				
	$\Delta\alpha = 2°$	$\Delta\alpha = 4°$	$\Delta\alpha = 6°$	$\Delta\alpha = 8°$	$\Delta\alpha = 10°$
79					
	-16.31				
81		-16.31			
	-16.31		-14.68		
83		-13.86		-14.68	
	-11.42		-14.14		-15.17
85		-13.05		-14.88	
	-14.68		-14.41		
87		-15.90			
	-17.13				
89					
90					
91					
	17.13				
93		15.90			
	14.68		14.41		
95		13.05		14.48	
	11.42		13.59		14.84
97		13.05		14.27	
	14.68		14.14		
99		15.49			
	16.31				
101					

Table 6.4: Calculated MAE of the absolute velocity of RBCs for all combinations of Doppler angles. δ is the set Doppler angle and $\Delta\alpha$ is the angle difference between the two detection directions.

δ (°)	MAE in (mm/s) at varible angle differences $\Delta\alpha$
	$\Delta\alpha = 2°$	$\Delta\alpha = 4°$	$\Delta\alpha = 6°$	$\Delta\alpha = 8°$	$\Delta\alpha = 10°$
79					
	3.09				
81		3.09			
	3.09		1.46		
83		0.64		1.46	
	-1.80		0.91		1.95
85		-0.17		1.66	
	1.46		1.19		
87		2.68			
	3.90				
89					
90					
91					
	3.90				
93		2.68			
	1.46		1.19		
95		-0.17		1.25	
	-1.80		0.37		1.62
97		-0.17		1.05	
	1.46		0.91		
99		2.27			
	3.09				
101					

7. Discussion

In this thesis, the DAQ program of the single detector measurement system provided by the Institute of Systems Engineering from the HES-SO Valais-Wallis was adapted towards its use for LDV measurements. The DAQ program was adapted by implementing new sub-VIs for evaluating and saving LDV measurements and adding the necessary controls, displays and indicators to the input- and measurement screen.

To validate the hardware and the changed DAQ program for the use of LDV measurements, in vitro measurement setups were assembled. For both measurement setups it is key, to determine the position of the rotary table where the Doppler angle δ is exactly 90°, i.e. the angle where no frequency shift is measured by the LDV system, because there is no component of $\vec{v}$ towards the measurement system. The first and more simple setup used a rotating disc as sample. In order to get repeatable results, the measurement point needs to be set between the lines of the disconnected circular grid imprinted on the paper cover of the rotating disc. Only if the surface plane of the rotating disc lies in the point of focus of the measurement system, the resulting spectrum has a narrow peak in the power spectrum and a clear frequency difference Δf_{max} can be measured. The linear slope k_v and the axis intercept d_v of the characteristic curve of the electric motor have to be determined exactly. Otherwise the calculated and the measured values can not be compared. The rotating disc setup provided proof that the hardware is in tact and the changed DAQ program provides the expected results anticipated by the theory of LDV.

The second setup used a capillary through which blood was pumped as a sample to provide an in vitro setup which is already near to an in vivo measurement. To make sure the maximum frequency difference Δf_{max} is measured, the measurement point needs to be set in the center of the capillary. The capillary must be in the measurement system's point of focus to get the characteristic shape of the power spectrum of a parabolic velocity profile and a clear cut-off becomes visible. Only then an exact determination of the maximum frequency difference Δf_{max} is possible. Also important for this measurement setup is an exact determination of the capillary diameter. With the capillary setup, the results of the first setup were confirmed. The measured frequency difference Δf_{max} generated through the frequency shift caused by the velocity of RBCs in the blood flow through the capillary can be linked to the theory of LDV.

The measurement results of the second setup were additionally interpreted towards

the possibility of measuring the absolute velocity of RBCs in retinal blood vessels in rat eyes with a two detector measurement system. The measured spectrum does not show a clear cut-off frequency if the detector is positioned at a Doppler angle between $87° < \delta < 93°$ and also for Doppler angles $\delta < 80°$ and $100° < \delta$ the cut-off is harder to determine. Therefore, the most promising Doppler angles are to be found in two intervals $80° < \delta < 87°$ or $93° < \delta < 100°$. The most promising results with the smallest MAE occur with an angle difference $\Delta\alpha = 4°$ between two detectors and a combination of the Doppler angles $\delta_1 = 83°$, $\delta_2 = 87°$ or $\delta_1 = 93°$, $\delta_2 = 97°$ or $\delta_1 = 95°$, $\delta_2 = 99°$. That corresponds to small angles between the incident laser beam and both detection directions of α_1 between 3-5° and α_2 between 7-9°. This result coincides with the prediction of the theory of LDV, where small angles α_1 and α_2 between the incident laser beam and the two detection directions are predicted. Since the angle between the incident laser beam and the second detection direction α_2 needs to be only $\sim 7°$, which is below the possible maximum entrance angle into a rat's eye of $\theta \sim 11°$, a LDV measurement system with two detectors and capable of measuring the absolute velocity of blood flow in retinal blood vessels of rat eyes seems to be possible.

8. Conclusion and Outlook

In conclusion, the adapted single detector measurement system provided by the Institute of Systems Engineering from the HES-SO Valais-Wallis is usable to measure the relative blood flow velocity via LDV. The anatomy of the rat eye, together with the results obtained from theory and experiments, suggest that bidirectional LDV is possible in the rat eye.
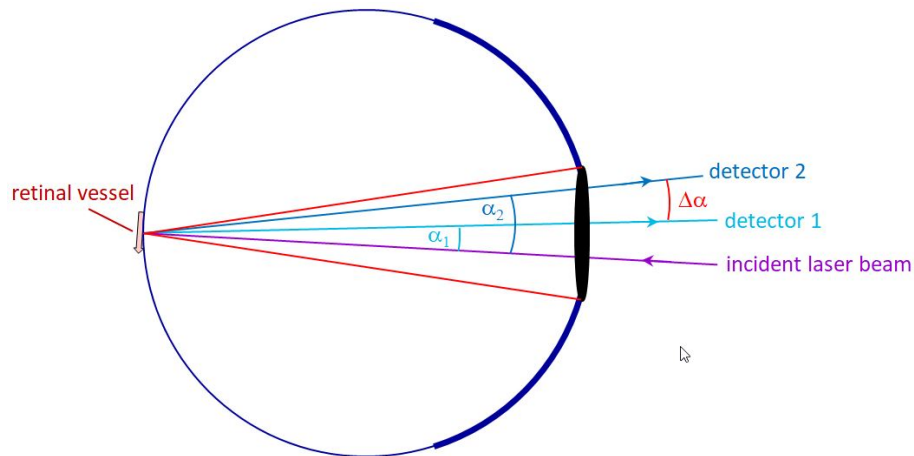

Figure 8.1: Schematic rat eye with incident laser beam and two detectors.

The first step towards such a system would be to automate the acquisition of the measured maximum frequency difference Δf_{max} (or cut-off frequency) of the spectrum in the DAQ program to guarantee user independent results and easier evaluation. Furthermore, the DAQ program has to be equipped with a second signal input for the second detector.

The hardware needs to provide a second detection direction for the second detector. The second detection direction can be provided by a right angle prism mirror that splits the light collected by the optical system into two detectors. Unfortunately the provided system does not offer a lot of room to include a second detector without further changes. Presumably, the easiest way would be to build a new measurement system already planned to include a second detector (Fig. 8.2).
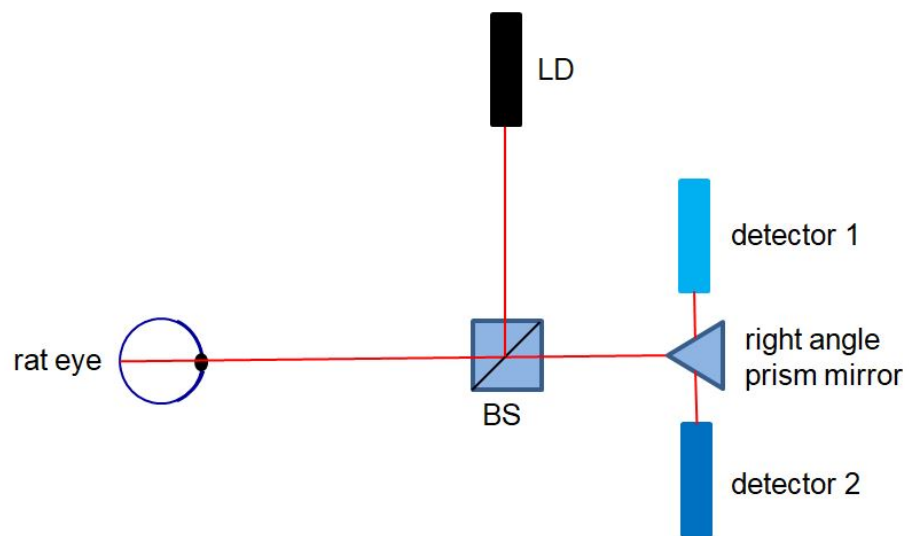
Figure 8.2: Schematic measurement system with a laser diode (LD), a beam splitter (BS), the rat eye as sample, the right angle prism mirror that splits the light into two detectors.

Bibliography

[1] D. Link, C. Strohmaier, B. U. Seifert, T. Riemer, H. A. Reitsamer, J. Haueisen, and W. Vilser. Novel non-contact retina camera for the rat and its application to dynamic retinal vessel analysis. *Biomed. Opt. Express*, 2(11):3094–3108, 2011. doi: 10.1364/BOE.2.003094.

[2] L. Schmetterer and J. Kiel. *Ocular Blood Flow*. Springer Berlin Heidelberg, 2012. doi: 10.1007/978-3-540-69469-4. 978-3-540-69468-7.

[3] M. Mentek, F. Truffer, C. Chiquet, D. Godin-Ribuot, S. Amoos, C. Loeuillet, M. Bernabei, and M. Geiser. Compact laser doppler flowmeter (ldf) fundus camera for the assessment of retinal blood perfusion in small animals. *PLOS ONE*, 10(7), 07 2015. doi: 10.1371/journal.pone.0134378.

[4] 04 2017. URL http://www.who.int/blindness/causes/priority/en/.

[5] B. Pemp and L. Schmetterer. Ocular blood flow in diabetes and age-related macular degeneration. *Canadian Journal of Ophthalmology*, 43(3):295–301, 2008. doi: 10.3129/i08-049.

[6] J. E. Grunwald, C. E. Riva, J. Baine, and A. J. Brucker. Total retinal volumetric blood low rate in diabetic patients with poor glycemic control. *Ophthalmology and Visual Science*, 33(2):356–363, 1992. URL http://www.iovs.org/content/33/2/356.abstract.

[7] A. Boltz, A. Luksch, B. Wimpissinger, N. Maar, G. Weigert, S. Frantal, W. Brannath, G. Garhöfer, E. Ergun, M. Stur, and L. Schmetterer. Choroidal blood flow and progression of age-related macular degeneration in the fellow eye in patients with unilateral choroidal neovascularization. *Invest. Ophthalmol. Vis. Sci.*, 51(8):4220–3225, 2010. doi: 10.1167/iovs.09-4968.

[8] G. C. Aschinger, L. Schmetterer, K. Fondi, V. Aranha Dos Santos, G. Seidel, G. Garhöfer, and R. M. Werkmeister. Effect of diffuse luminance flicker light stimulation on total retinal blood flow assessed with dual-beam bidirectional doppler oct. *Invest. Ophthalmol. Vis. Sci.*, 58:1167–1178, 2017. doi: 10.1167/iovs.16-20598.

[9] J.A. Ketterling, R. Urs, and R.H. Silverman. In vivo imaging of ocular blood flow using high-speed ultrasound. *IEEE International Ultrasonics Symposium*, 2016. doi: 10.1109/ULTSYM.2016.7728578.

[10] V. Doblhoff-Dier, L. Schmetterer, W. Vilser, G. Garhöfer, M. Gröschl, R. A. Leitgeb, and R. M. Werkmeister. Measurement of the total retinal blood flow using dual beam fourier-domain doppler optical coherence tomography with orthogonal detection planes. *Biomedical Optics Express*, 5(2):630–642, 2014. doi: 10.1364/BOE.5.000630.

[11] C. Gao, Q. Wang, G. Wei, and X. Long. A highly accurate calibration method for terrestrial laser doppler velocimeter. *IEEE TRANSACTIONS ON BIOMEDICAL ENGINEERING*, pages 1–10, 2017. doi: 10.1109/TIM.2017.2685078.

[12] S. Chinde, N. Dumala, M. F. Rahman, S. S. K. Kamal, S. I. Kumari, M. Mahboob, and P. Grover. Toxicological assessment of tungsten oxide nanoparticles in rats after acute oral exposure. *Environ Sci Pollut Res*, 2017. doi: 10.1007/s11356-017-8892-x.

[13] URL https://wissenschaft.bmwfw.gv.at/bmwfw/ministerium/veranstaltungenpublikationen/publikationen/forschung/statistiken/tierversuchsstatistiken/.

[14] 05 2017. URL https://www.hevs.ch/de/.

[15] T. G. M. F. Gorgels and D. van Norren. "Spectral transmittance of the rat lens". *Vision Research*, 32(8):1509–1512, 1992.

[16] A. Hughes. A schematic eye for the rat. *Vision Research*, 19(5):569–588, 1979. doi: 10.1016/0042-6989(79)90143-3.

[17] URL http://prometheus.med.utah.edu/~marclab/eyes.pdf.

[18] M. T. Block. Note on the refraction and image formation of the rat's eye. *Vision Research*, 9(6):705–711, 1969. doi: 10.1016/0042-6989(69)90127-8.

[19] S. D. Wajer, M. Taomoto, D. Scott McLeod, R. L. McCally, H. Nishiwaki, M. E. Fabry, R. L. Nagel, and G. A. Lutty. Velocity measurements of normal and sickle red blood cells in the rat retinal and choroidal vasculatures. *Microvascular Research*, 60:281–293, 2000. doi: 10.1006/mvre.2000.2270.

[20] I. A. Bhutto. Retinal vascular changes during aging in wistar kyoto rats. *Ophthalmic Res*, 27:249–261, 1995. doi: 10.1159/000267734.

[21] H. Ninomiya and H. Kuno. Microvasculature of the rat eye: scannin electron microscopy of vascular corrosion casts. *Veterinary Ophthalmology*, 4:55–59, 2001. doi: 10.1046/j.1463-5224.2001.00143.x.

[22] C.E. Riva, G.T. Feke, B. Eberli, and V. Benary. Bidirectional ldv system for absolute measurement of blood speed in retinal vessels. *Applied Op*, 18(13): 2301–2306, 07 1979.

[23] W. Drexler and J. G. Fujimoto. *"Optical Coherence Tomography"*. Springer International Publishing Switzerland, Berlin, Heidelberg, New York, 2 edition, 2015. ISBN 978-3-540-77549-2. doi: 10.1007/978-3-319-06419-2.

[24] V. Doblhoff-Dier. *"Determination of the Total Retinal Blood Flow Using Fourier-Domain Optical Coherence Tomography and Fundus Imaging"*. Dissertation, Technische Universität Wien, 2014.

[25] W. Demtröder. *Demtröder Experimentalphysik 2 - Elektrizität und Optik*. Number 2 in Demtröder Experimentalphysik. Springer, 5 edition, 2009. doi: 10.1007/978-3-540-68219-6. ISBN 978-3-540-68210-3.

[26] C. K. Hitzenberger, M. Danner, W. Drexler, and A. F. Fercher. Measurement of the spatial coherence of superluminescent diodes. *Journal of Modern Optics*, 46(12):1763–1774, 1999. doi: 10.1080/09500349908231370. URL `http://www.tandfonline.com/doi/abs/10.1080/09500349908231370`.

[27] Rüdiger Paschotta. Rp photonicsencyclopedia, 07 2017. URL `https://www.rp-photonics.com/coherence.html`.

[28] W. Demtröder. *Demtröder Experimentalphysik 1 - Mechanik und Wärme*. Number 1 in Demtröder Experimentalphysik. Springer, 5 edition, 2008. doi: 10.1007/978-3-540-79295-6. ISBN 978-3-540-79294-9.

[29] Y. Yeh and H. Z. Cummins. Localized fluid flow measurements with an he-ne laser spectrometer. *Appl. Phys. Lett.*, 4(176), May 1964. doi: 10.1063/1.1753925.

[30] C.E. Riva and G.T. Feke. *The Biomedical Laser: Technology and Clinical Applications*. Springer-Verlag New York Inc., 1 edition, 1981. doi: 10.1007/978-1-4612-5922-0. ISBN-13:978-1-4612-5924-4.

[31] C. E. Riva, B. Ross, and G. B. Benedek. Laser doppler measurements of blood flow in capillary tubes and retinal arteries. *Invest. Ophthalmol. Vis. Sci.*, 11 (11):936–944, 11 1972.

[32] T. Tanaka and G. B. Benedek. Measurement of the velocity of blood flow (in vivo) using a fiber optic catheter and optical mixing spectroscopy. *Applied Optics*, 14(1):189–196, January 1974.

[33] G.T. Feke, D. G. Goger, H. Tagawa, and F. C. Delori. Laser doppler technique for absolute measurement of blood speed in retinal vessels. *IEEE TRANSACTIONS ON BIOMEDICAL ENGINEERING*, BME-34(9):673–800, 1987.

[34] C. E. Riva, J. E. Grunwald, S. H. Sinclair, and K. O'Keefe. Fundus camera based retinal ldv. *Applied Optics*, 20(1):117–120, 1 1981. doi: 10.1364/AO.20.000117.

[35] C. E. Riva, J. E. Grunwald, and B. L. Petrig. Laser doppler measurement of retinal blood velocity: validity of the single scattering model. *Applied Optics*, 24(5):605–607, 3 1985. doi: 10.1364/AO.24.000605.

[36] L. M. Rapp, B. L. Tolman, and H. S. Dhindso. Separate mechanisms for retinal damage by ultraviolet-a and mid-visible light. *Invest. Ophthalmol. Vis. Sci.*, 31 (6):1186–1190, 1990.

[37] 07 2017. URL https://www.thorlabs.de/newgrouppage9.cfm?objectgroup_id=897.

[38] 08 2017. URL http://www.ni.com/tutorial/4342/en/.

[39] 08 2017. URL http://www.ni.com/download/traditional-ni-daq-legacy-7.4.1/586/en/.

[40] V. Dovgal. *Optical Methods for Investigations of Structural Changes In Paper During Drying*. PhD thesis, TU Darmstadt, 2013.

[41] R. Werkmeister. *Dual-beam Bidirectional Doppler Fourier-Domain Optical Coherence Tomography*. PhD thesis, Medical University of Vienna, 2010.

[42] H. Li, L. Lin, and S. Xie. Refractive index of human whole blood with different types in the visible and near-infrared ranges. *Proc.SPIE*, 3914:517–521, 2000. doi: 10.1117/12.388073.